

Figure 1 Effects of nutlin-3 on proliferation, migration, and p53 pathways in VSMCs. (A) VSMCs pretreated with nutlin-3 for 6 h were stimulated with PDGF-BB (50 ng/mL) for 24 h and [³H]-thymidine incorporation was counted. * $P < 0.05$, ** $P < 0.01$ vs. PDGF(-)-Nutlin-3(-); † $P < 0.05$, †† $P < 0.01$ vs. PDGF(+)-Nutlin-3(-) ($n = 3$). (B) Effects of nutlin-3 on VSMC migration by *in vitro* scratch assay. VSMC monolayers were scratched and then stimulated with PDGF-BB (50 ng/mL) for 24 h in the presence or absence of nutlin-3. Nuclei were stained with DAPI. Representative microphotographs and the quantitative analysis are shown. * $P < 0.005$ vs. control, † $P < 0.05$ vs. PDGF ($n = 3$). (C) The expression levels of p53, p21, and MDM2 in VSMCs stimulated with nutlin-3 (10 μmol/L) were assessed by western blot analysis. Histone H3 was used for loading control. The same results were obtained in three other independent experiments. (D) The effect of nutlin-3 on VSMC apoptosis was analysed by flow cytometry. After pretreatment with nutlin-3 (10 μmol/L) for 24 h and incubation with H₂O₂ (5 mmol/L) for 1 h, VSMCs were stained with PI and Annexin V-FITC. The percentage of apoptotic cells (Annexin V-positive and PI-negative fraction) is shown. n.s.: not significant ($n = 3$). Values represent mean ± SEM.

in each group, suggesting that there would not be differences in collagen fibre properties affecting tissue stability (Figure 3D). Immunostaining of PECAM-1 showed that the luminal surface of the neointima was overlaid with endothelial cells in both control and nutlin-3 groups, indicating that administration of nutlin-3 did not impair re-endothelialization (Figure 3E). These results suggest that treatment with nutlin-3 attenuates neointimal overgrowth without affecting vascular tissue integrity. Expression of p53 and p21 was up-regulated in the vascular tissues of nutlin-3-administered mice compared with untreated mice (Figure 3F). MDM2 expression was unaffected by treatment with nutlin-3 (Figure 3F).

3.4 Effects of MDM2 inhibition on vascular proliferation and inflammation

Incorporation of BrdU into the neointima cells was decreased in nutlin-3-treated mice compared with control mice at 14 days but not 28 days after vascular injury (Figure 4A). There were only a few TUNEL-positive apoptotic cells detected at 7 days after injury, however, enhanced apoptosis was not observed in nutlin-3-administered mice (Figure 4B). TUNEL-positive cells were not detected either in control or nutlin-3 groups at 14 and 28 days after injury (Figure 4B). These results suggest minor contribution of

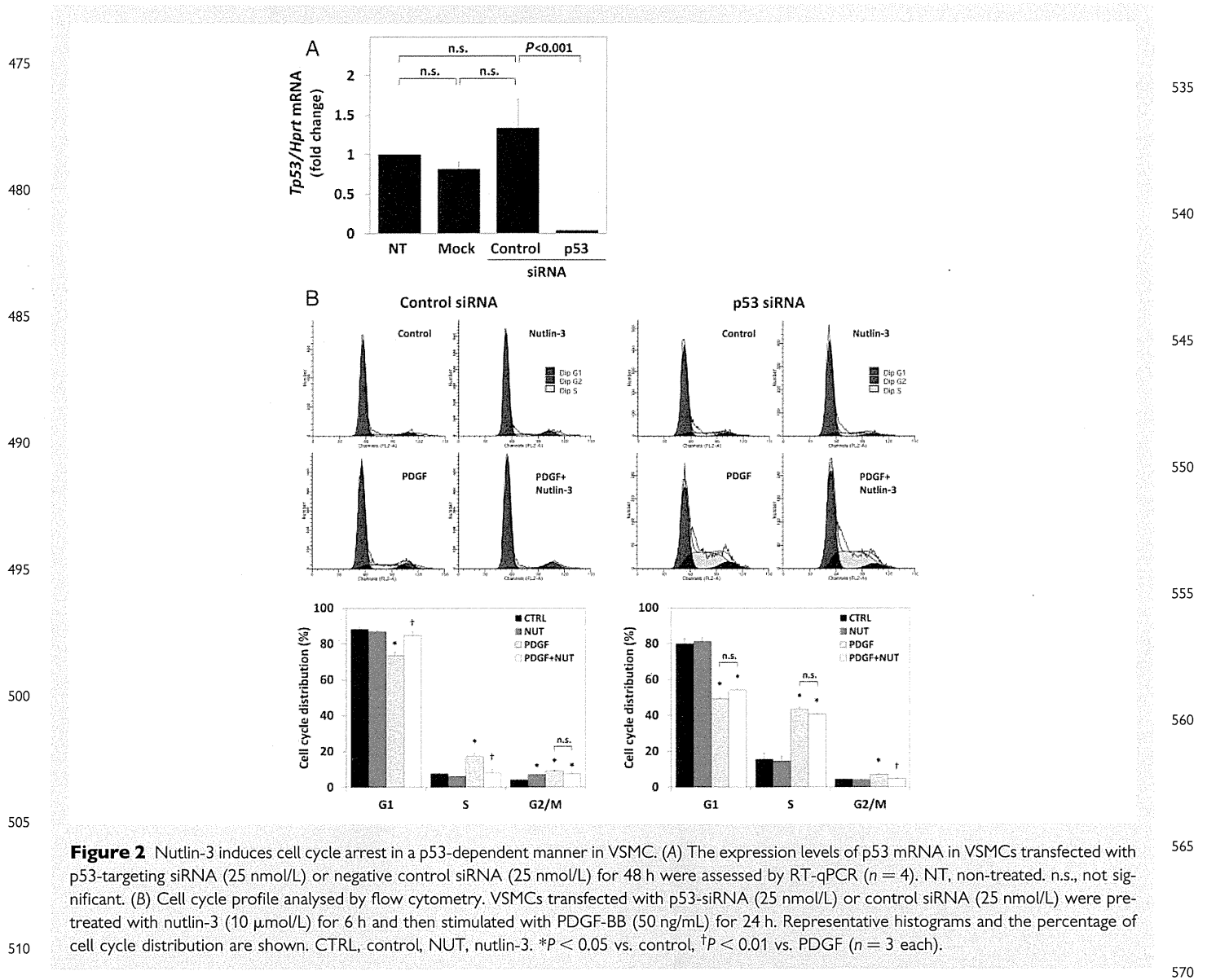


Figure 2 Nutlin-3 induces cell cycle arrest in a p53-dependent manner in VSMC. (A) The expression levels of p53 mRNA in VSMCs transfected with p53-targeting siRNA (25 nmol/L) or negative control siRNA (25 nmol/L) for 48 h were assessed by RT-qPCR ($n = 4$). NT, non-treated. n.s., not significant. (B) Cell cycle profile analysed by flow cytometry. VSMCs transfected with p53-siRNA (25 nmol/L) or control siRNA (25 nmol/L) were pre-treated with nutlin-3 (10 $\mu\text{mol/L}$) for 6 h and then stimulated with PDGF-BB (50 ng/mL) for 24 h. Representative histograms and the percentage of cell cycle distribution are shown. CTRL, control, NUT, nutlin-3. * $P < 0.05$ vs. control, $^{\dagger}P < 0.01$ vs. PDGF ($n = 3$ each).

apoptosis to the inhibition of neointimal growth by nutlin-3. Vascular inflammation is mainly regulated by NF- κ B-dependent gene transcription,²² and involved in the progression of vascular proliferative diseases.^{1–3} Since it has been reported that p53 inhibits NF- κ B pathway,^{23–27} we also investigated whether nutlin-3 affects NF- κ B-regulated gene expression and infiltration of inflammatory cells in injured vascular tissues. Infiltration of macrophages and T-lymphocytes in the injured vessels was significantly attenuated in nutlin-3-administered mice (Figure 4C and D). RT-qPCR of the injured vessels showed that mRNA expression of NF- κ B-regulated genes including chemokine (C-C motif) ligand 5 (CCL5), interleukin-6 (IL-6), and intercellular adhesion molecule-1 (ICAM-1) was suppressed in nutlin-3-treated mice (Figure 5A).

3.5 Nutlin-3 suppression of nuclear activation of NF- κ B is dependent on p53

To elucidate the mechanism of the decrease in proinflammatory gene expression in the injured vessels of nutlin-3-treated mice, we performed

NF- κ B DNA-binding ELISA using cultured rat VSMCs. Treatment with nutlin-3 significantly attenuated NF- κ B activation induced by TNF α in VSMCs transfected with control siRNA (Figure 5B), while this inhibitory effect was abrogated in VSMCs transfected with p53-targeting siRNA (Figure 5B). The NF- κ B-suppressing effect of nutlin-3 was also abolished in p53-deficient mouse VSMCs (Supplementary material online, Figure S3). These results suggest that the inhibitory effect of nutlin-3 on NF- κ B activation depends on p53.

4. Discussion

In the present study, we demonstrated that an MDM2 inhibitor nutlin-3 suppressed VSMC proliferation through cell cycle arrest at G1 phase. The effects of nutlin-3 depend on p53 because nutlin-3 failed to show any effects on VSMCs transfected with p53-targeting siRNA and p53-deficient VSMCs. We also demonstrated that treatment with nutlin-3 attenuated neointimal hyperplasia after vascular injury without increasing vascular tissue vulnerability. Inhibition of

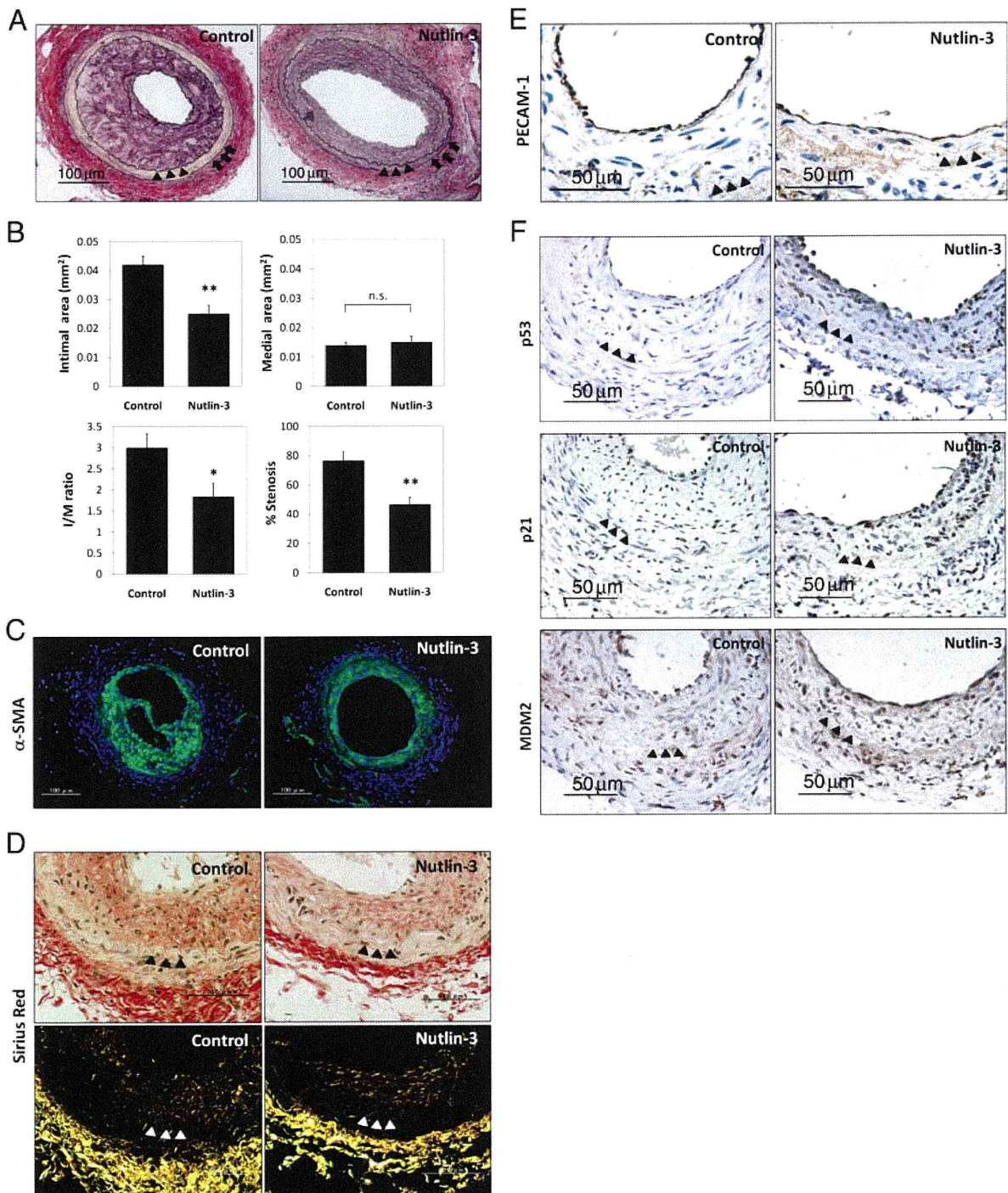


Figure 3 Nutlin-3 attenuates neointimal hyperplasia after vascular injury. (A) Femoral arteries at 28 days after vascular injury (elastica van Gieson staining). Arrows indicate external elastic lamina. Arrowheads indicate internal elastic lamina. (B) Intimal area, medial area, intima/media (I/M) area ratio, and percent stenosis at 28 days after injury were analysed. Values represent mean \pm SEM. * $P < 0.05$ vs. control, ** $P < 0.01$ vs. control (control, $n = 9$, nutlin-3, $n = 7$). (C) Wire-injured arteries (28 days) stained with FITC-conjugated anti- α -SMA antibody. Green, α -SMA. Blue, nuclei (DAPI). (D) Sirius red staining of injured vessels (28 days). Collagen fibres were stained in red (upper panels). The sirius red-stained tissue specimens identical to upper panels were observed by polarizing microscopy (lower panels). (E) Immunostaining of PECAM-1 in vascular tissues at 28 days after injury. (F) Immunostaining of p53, p21, and MDM2 in the injured vessels (28 days). The same results were obtained in other samples (control, $n = 9$, nutlin-3, $n = 7$).

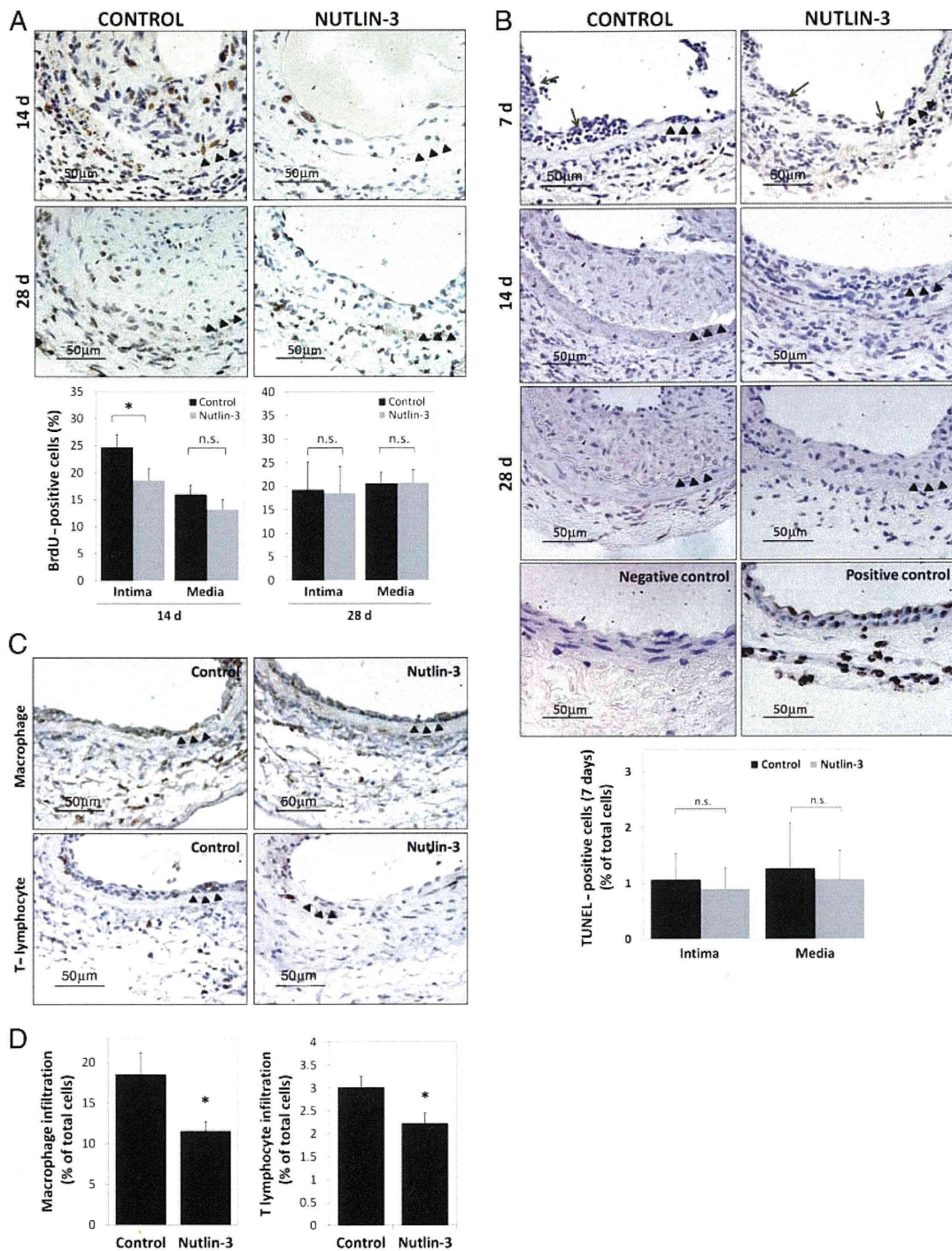


Figure 4 Modulation of vascular proliferation and inflammatory responses by MDM2 inhibition. (A) Cell proliferation was assessed by BrdU incorporation at 14 and 28 days after vascular injury. (Upper) Representative micrographs are shown. Arrowheads indicate internal elastic lamina. (Lower) Quantitative analysis of BrdU-positive cells in the neointima and the media. * $P < 0.05$. n.s.: not significant. (14 days: control, $n = 15$, nutlin-3, $n = 11$; 28 days: control, $n = 9$, nutlin-3, $n = 7$). (B) (Upper) Apoptotic cells assessed by TUNEL method at 7, 14, and 28 days after injury. Arrows indicate TUNEL-positive cells. Positive control was the tissue specimen biochemically treated with DNase I, while negative control was the specimen incubated without TdT. (Lower) Quantitative analysis of TUNEL-positive cells in the neointima and the media at 7 days after injury. n.s., not significant (control, $n = 7$, nutlin-3, $n = 8$). (C) Infiltration of inflammatory cells at 7 days after vascular injury. Macrophages were immunostained with anti-Mac-3 antibody. T-lymphocytes were stained with anti-CD3 antibody. (D) Quantitative analysis of the number of inflammatory cells which infiltrated per section. * $P < 0.05$ vs. control ($n = 5$ each).

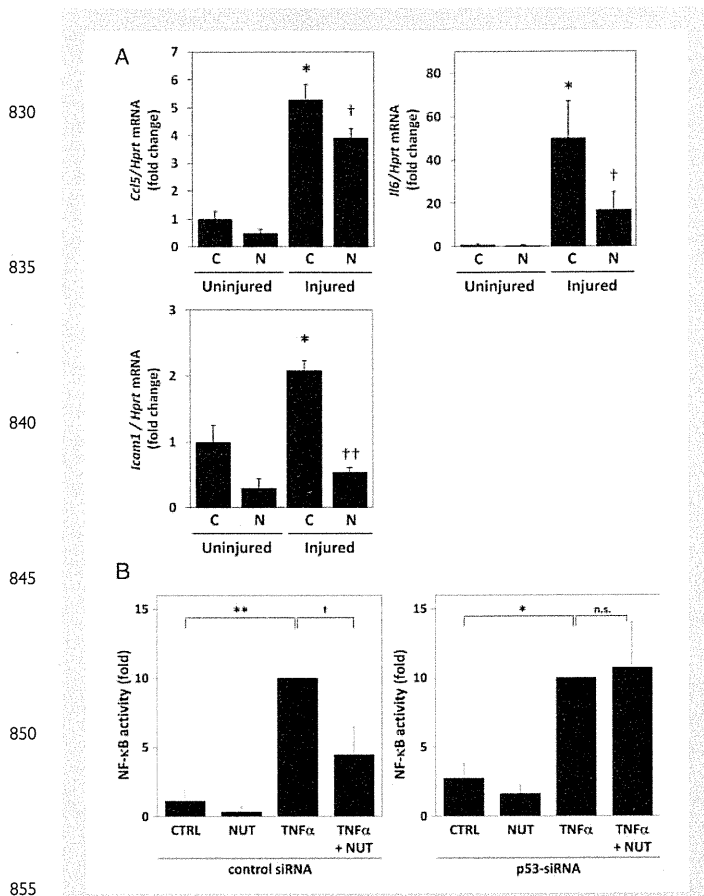


Figure 5 Effects of MDM2 inhibition on inflammatory gene expression and NF- κ B transcriptional activity. (A) mRNA expression levels of CCL5, IL-6, and ICAM-1 at 7 days after vascular injury were determined by RT-qPCR. C, control; N, nutlin-3. * $P < 0.005$ vs. control (uninjured); † $P < 0.05$, †† $P < 0.01$ vs. control (injured) (control, $n = 10$, nutlin-3, $n = 10$). Values represent mean \pm SEM. (B) Effect of nutlin-3 on NF- κ B transactivation in VSMCs was assessed by DNA-binding ELISA for NF- κ B p65. VSMCs transfected with control siRNA or p53-siRNA were stimulated with TNF α (20 ng/mL) for 1 h after pretreatment with nutlin-3 (10 μ mol/L) for 24 h ($n = 3$ each). Values represent mean \pm SEM. CTRL, control; NUT, nutlin-3. * $P < 0.05$, ** $P < 0.001$ vs. control, † $P < 0.05$ vs. TNF α , n.s., not significant ($n = 3$).

vascular cell proliferation, inflammatory cell infiltration, and proinflammatory gene expression was observed in the injured vessels of nutlin-3-administered mice, suggesting that nutlin-3 ameliorated maladaptive vascular remodelling through inhibition of neointimal VSMC growth and modulation of inflammatory process. Infiltration of leukocytes mediated by chemokines and VSMC proliferation are critical to neointimal growth after vascular injury.³ Therefore, a therapeutic strategy against both cell proliferation and vascular inflammation is rational for efficacious remedy for neointimal hyperplasia. MDM2 inhibitors may have unique therapeutic potential because it is capable of inhibiting NF- κ B activation as well as inducing cell-cycle arrest via p53 activation.

Previous reports have demonstrated that the protective role of p53 against neointimal hyperplasia.^{28–34} Such an effect has been thought to be brought about by increased apoptosis or inhibition of

proliferation of VSMCs. These studies adopted, however, p53 gene transfer by adenovirus vectors, liposome, or transgenic technique, which are technically and ethically difficult to utilize in the clinical settings. Indeed p53 activation can be instigated by anticancer drugs, which is inevitably associated with DNA damage leading to enhanced apoptosis and tissue damage.¹⁵ The fact that nutlin-3 can activate p53 by inhibition of MDM2, not by DNA damage-triggered induction, encourages us to apply the 'p53 activation' to the conquest of vascular proliferative diseases practically.

Since MDM2 is a downstream target gene of p53 as well as p21, MDM2 up-regulation by treatment with MDM2 inhibitor nutlin-3 is thought to result from a negative feedback mechanism. Although the kinetics of p53, p21, and MDM2 in VSMCs seems parallel in time in our results, up-regulation of p21 and MDM2 may follow the induction of p53 in a delayed fashion at the early phase after stimulation with nutlin-3 like seen in other cells.^{18,19}

Nutlin-3 inhibits cell proliferation by p53 activation leading to p21-mediated cell cycle arrest at G1 phase. p53 can also induce apoptosis in response to stress signals, but apoptosis-inducing effect of p53 might depend on cell type or require further cofactors or modifications.³⁵ Nutlin-3 does not induce apoptosis of vascular endothelial cells,³⁶ neutrophils, and macrophages.²³ In this study, acceleration of apoptosis was not observed either in nutlin-3-treated VSMCs or neointima of nutlin-3-administered mice after vascular injury, which is consistent with previous studies. Very early apoptosis after vascular injury is relevant for vascular remodelling. SMC apoptosis is induced immediately after vascular injury, attaining to the peak in 0.5–1 h, and declines rapidly.³⁷ Considering the fact that administration of nutlin-3 was instituted by implantation of mini-osmotic pumps following vascular injury and the concentration of nutlin-3 would reach steady state for at least several hours, it is unlikely that nutlin-3 affects apoptosis which occurs very early after vascular injury in our models.

p53 activation is known to suppress NF- κ B-dependent gene expression.^{23–25} It has been reported that p53 and NF- κ B can repress the transactivation of each other via competition for transcriptional co-activator p300/CREB-binding protein (CBP).^{26,27} We showed that nutlin-3 suppressed NF- κ B activation in VSMCs. Though a direct proof of NF- κ B activation is lacking in our animal experiments, inhibition of the expression of NF- κ B-regulated proinflammatory genes, such as CCL5, IL-6, and ICAM-1, suggests that nutlin-3 may suppress NF- κ B activation in injured vessels as shown in cultured VSMCs. These observations about the effects of MDM2 inhibitor beyond anti-proliferation, that is, anti-inflammatory activities, implicate that it may be applicable to the treatment of atherosclerotic vascular diseases as well as post-intervention restenosis.

In the present study, we did not investigate the mechanism by which nutlin-3 suppressed VSMC migration. Nutlin-3 inhibits cancer cell migration via cytoskeletal rearrangement in a p53-dependent manner.³⁸ Reportedly, p53 inhibits cell migration by regulation of Cdc42 and Rac1 pathways.^{39,40} While we speculate that nutlin-3 inhibits VSMC migration through p53-mediated suppression of Rho GTPases, further examination is required.

The limitation of the present study is that we did not verify the effects of nutlin-3 on neointima formation in p53-deficient mice to establish the definite link between the effects of nutlin-3 and p53 *in vivo*. However, we observed that nutlin-3 failed to inhibit cell cycle progression and NF- κ B activation in p53-knocked down

945 VSMCs and p53-deficient VSMCs, strongly suggesting that the effects
of nutlin-3 depend on p53. Furthermore, there are many reports
demonstrating that *in vivo* administration of nutlin-3 suppressed the
growth of tumours with wild-type p53, whereas treatment with
nutlin-3 did not affect the growth of p53-deficient or mutant
950 p53-bearing tumours in mice.^{17,18,41} These findings including our
results suggest that the pharmacological action of nutlin-3 *in vivo* is
dependent on p53 as well. For another point, we cannot exclude
possible secondary effects of nutlin-3 on neointima formation by
way of, for example, inhibition of systemic cytokine expression and
955 direct inhibitory effects on inflammatory cells such as macrophages
and leukocytes. Further investigations are required on this point.

In conclusion, p53 activation by MDM2 inhibition prevented cellular
proliferation, migration, and NF- κ B activation in VSMCs; and besides
attenuated neointimal hyperplasia with prevention of vascular pro-
960 liferation and inflammatory responses. Targeting MDM2-p53 inter-
action might be a novel therapeutic strategy for treatment of
vascular proliferative diseases.

Supplementary material

965 Supplementary material is available at *Cardiovascular Research* online.

Acknowledgements

We thank the Research Support Centre, Kyushu University Graduate
970 School of Medical Sciences for technical supports.

Conflict of interest: none declared.

Funding

975 This work was supported in part by Grants-in-Aid for Scientific Research
from the Ministry of Education, Culture, Sports, Science, and Technology
of Japan (19590867).

References

- Libby P. Inflammation in atherosclerosis. *Nature* 2002;**420**:868–874.
- Dzau VJ, Braun-Dullaeus RC, Sedding DG. Vascular proliferation and atherosclerosis: new perspectives and therapeutic strategies. *Nat Med* 2002;**8**:1249–1256.
- Costa MA, Simon DI. Molecular basis of restenosis and drug-eluting stents. *Circulation* 2005;**111**:2257–2273.
- Riley T, Sontag E, Chen P, Levine A. Transcriptional control of human p53-regulated genes. *Nat Rev Mol Cell Biol* 2008;**9**:402–412.
- Guevara NV, Kim HS, Antonova EI, Chan L. The absence of p53 accelerates atherosclerosis by increasing cell proliferation *in vivo*. *Nat Med* 1999;**5**:335–339.
- van Vlijmen BJ, Gerritsen G, Franken AL, Boesten LS, Kockx MM, Gijbels MJ *et al*. Macrophage p53 deficiency leads to enhanced atherosclerosis in APOE*3-Leiden transgenic mice. *Circ Res* 2001;**88**:780–786.
- Merched AJ, Williams E, Chan L. Macrophage-specific p53 expression plays a crucial role in atherosclerosis development and plaque remodeling. *Arterioscler Thromb Vasc Biol* 2003;**23**:1608–1614.
- 980 Mercer J, Figg N, Stoneman V, Braganza D, Bennett MR. Endogenous p53 protects vascular smooth muscle cells from apoptosis and reduces atherosclerosis in ApoE knockout mice. *Circ Res* 2005;**96**:667–674.
- von der Thüsen JH, van Vlijmen BJ, Hoeben RC, Kockx MM, Havekes LM, van Berkel TJ *et al*. Induction of atherosclerotic plaque rupture in apolipoprotein E-/- mice after adenovirus-mediated transfer of p53. *Circulation* 2002;**105**:2064–2070.
- 985 Toledo F, Wahl GM. MDM2 and MDM4: p53 regulators as targets in anticancer therapy. *Int J Biochem Cell Biol* 2007;**39**:1476–1482.
- Toledo F, Wahl GM. Regulating the p53 pathway: *in vitro* hypotheses, *in vivo* veritas. *Nat Rev Cancer* 2006;**6**:909–923.
- Ihling C, Haendeler J, Menzel G, Hess RD, Fraedrich G, Schaefer HE *et al*. Co-expression of p53 and MDM2 in human atherosclerosis: implications for the regulation of cellularity of atherosclerotic lesions. *J Pathol* 1998;**185**:303–312.
- 1000 Nakamura Y, Suzuki S, Suzuki T, Ono K, Miura I, Satoh F *et al*. MDM2: a novel mineralocorticoid-responsive gene involved in aldosterone-induced human vascular structural remodeling. *Am J Pathol* 2006;**169**:362–371.
- Vassilev LT, Vu BT, Graves B, Carvajal D, Podlaski F, Filipovic Z *et al*. *In vivo* activation of the p53 pathway by small-molecule antagonists of MDM2. *Science* 2004;**303**:844–848.
- Vassilev LT. MDM2 inhibitors for cancer therapy. *Trends Mol Med* 2007;**13**:23–31.
- Sarek G, Kurki S, Enback J, Iotzova G, Haas J, Laakkonen P *et al*. Reactivation of the p53 pathway as a treatment modality for KSHV-induced lymphomas. *J Clin Invest* 2007;**117**:1019–1028.
- 1010 Van Maerken T, Ferdinande L, Taildeman J, Lambertz I, Yigit N, Verduyck L *et al*. Antitumor activity of the selective MDM2 antagonist nutlin-3 against chemoresistant neuroblastoma with wild-type p53. *J Natl Cancer Inst* 2009;**101**:1562–1574.
- Tovar C, Rosinski J, Filipovic Z, Higgins B, Kolinsky K, Hilton H *et al*. Small-molecule MDM2 antagonists reveal aberrant p53 signaling in cancer: implications for therapy. *Proc Natl Acad Sci USA* 2006;**103**:1888–1893.
- Endo S, Yamato K, Hirai S, Moriwaki T, Fukuda K, Suzuki H *et al*. Potent *in vitro* and *in vivo* antitumor effects of MDM2 inhibitor nutlin-3 in gastric cancer cells. *Cancer Sci* 2011;**102**:605–613.
- 1015 Sata M, Maejima Y, Adachi F, Fukino K, Saiura A, Sugiura S *et al*. A mouse model of vascular injury that induces rapid onset of medial cell apoptosis followed by reproducible neointimal hyperplasia. *J Mol Cell Cardiol* 2000;**32**:2097–2104.
- Andrae J, Gallini R, Betsholtz C. Role of platelet-derived growth factors in physiology and medicine. *Genes Dev* 2008;**22**:1276–1312.
- de Winther MP, Kanters E, Kraal G, Hofker MH. Nuclear factor κ B signaling in atherogenesis. *Arterioscler Thromb Vasc Biol* 2005;**25**:904–914.
- 1020 Liu G, Park YJ, Tsuruta Y, Lorne E, Abraham E. p53 Attenuates lipopolysaccharide-induced NF- κ B activation and acute lung injury. *J Immunol* 2009;**182**:5063–5071.
- Dey A, Wong ET, Bist P, Tergaonkar V, Lane DP. Nutlin-3 inhibits the NF κ B pathway in a p53-dependent manner: implications in lung cancer therapy. *Cell Cycle* 2007;**6**:2178–2185.
- Secchiero P, Corallini F, Rimondi E, Chiaruttini C, di lasio MG, Rustighi A *et al*. Activation of the p53 pathway down-regulates the osteoprotegerin expression and release by vascular endothelial cells. *Blood* 2008;**111**:1287–1294.
- 1025 Wadgaonkar R, Phelps KM, Haque Z, Williams AJ, Silverman ES, Collins T. CREB-binding protein is a nuclear integrator of nuclear factor- κ B and p53 signaling. *J Biol Chem* 1999;**274**:1879–1882.
- Webster GA, Perkins ND. Transcriptional cross talk between NF- κ B and p53. *Mol Cell Biol* 1999;**19**:3485–3495.
- Yonemitsu Y, Kaneda Y, Tanaka S, Nakashima Y, Komori K, Sugimachi K *et al*. Transfer of wild-type p53 gene effectively inhibits vascular smooth muscle cell proliferation *in vitro* and *in vivo*. *Circ Res* 1998;**82**:147–156.
- 1030 Matsushita H, Morishita R, Aoki M, Tomita N, Taniyama Y, Nakagami H *et al*. Transfection of antisense p53 tumor suppressor gene oligodeoxynucleotides into rat carotid artery results in abnormal growth of vascular smooth muscle cells. *Circulation* 2000;**101**:1447–1452.
- George SJ, Angelini GD, Capogrossi MC, Baker AH. Wild-type p53 gene transfer inhibits neointima formation in human saphenous vein by modulation of smooth muscle cell migration and induction of apoptosis. *Gene Ther* 2001;**8**:668–676.
- 1040 Mayr U, Mayr M, Li C, Wernig F, Dietrich H, Hu Y *et al*. Loss of p53 accelerates neointimal lesions of vein bypass grafts in mice. *Circ Res* 2002;**90**:197–204.
- Sata M, Tanaka K, Ishizaka N, Hirata Y, Nagai R. Absence of p53 leads to accelerated neointimal hyperplasia after vascular injury. *Arterioscler Thromb Vasc Biol* 2003;**23**:1548–1552.
- Wan S, George SJ, Nicklin SA, Yim AP, Baker AH. Overexpression of p53 increases lumen size and blocks neointima formation in porcine interposition vein grafts. *Mol Ther* 2004;**9**:689–698.
- 1045 Sanz-González SM, Barquín L, García-Cao I, Roque M, González JM, Fuster JJ *et al*. Increased p53 gene dosage reduces neointimal thickening induced by mechanical injury but has no effect on native atherosclerosis. *Cardiovasc Res* 2007;**75**:803–812.
- Aylon Y, Oren M. Living with p53, dying of p53. *Cell* 2007;**130**:597–600.
- Secchiero P, Corallini F, Gonelli A, Dell'Eva R, Vitale M, Capitani S *et al*. Antiangiogenic activity of the MDM2 antagonist nutlin-3. *Circ Res* 2007;**100**:61–69.
- 1050 Perlman H, Maillard L, Krasinski K, Walsh K. Evidence for the rapid onset of apoptosis in medial smooth muscle cells after balloon injury. *Circulation* 1997;**95**:981–987.
- Moran DM, Maki CG. Nutlin-3a induces cytoskeletal rearrangement and inhibits the migration and invasion capacity of p53 wild-type cancer cells. *Mol Cancer Ther* 2010;**9**:895–905.
- 1055 Gadea G, Lapasset L, Gauthier-Rouviere C, Roux P. Regulation of Cdc42-mediated morphological effects: a novel function for p53. *Embo J* 2002;**21**:2373–2382.
- Guo F, Gao Y, Wang L, Zheng Y. p19Arf-p53 tumor suppressor pathway regulates cell motility by suppression of phosphoinositide 3-kinase and Rac1 GTPase activities. *J Biol Chem* 2003;**278**:14414–14419.
- 1060 Sur S, Pagliarini R, Bunz F, Rago C, Diaz LA Jr., Kinzler KW *et al*. A panel of isogenic human cancer cells suggests a therapeutic approach for cancers with inactivated p53. *Proc Natl Acad Sci USA* 2009;**106**:3964–3969.

Peak Systolic Mitral Annulus Velocity Reflects the Status of Ventricular-Arterial Coupling—Theoretical and Experimental Analyses

Kazunori Uemura, MD, PhD, Toru Kawada, MD, PhD, Kenji Sunagawa, MD, PhD, and Masaru Sugimachi, MD, PhD, *Suita and Fukuoka, Japan*

Background: Peak systolic mitral annular velocity (S_m) measured by tissue Doppler echocardiography has been recognized as an independent predictor of mortality in patients with heart failure and in the general population. However, the mechanical determinants of S_m remain poorly defined.

Methods: A theoretical model of S_m was derived, which indicates that S_m is affected positively by left ventricular (LV) contractility and preload and inversely by LV afterload and ejection time (EJT). In 16 anesthetized dogs, S_m , LV volume, and LV pressure were measured using sonomicrometry and catheter-tip micromanometry. LV contractility, preload, and afterload were indexed by the end-systolic pressure/volume ratio (E_{es}'), end-diastolic volume (V_{ed}), and effective arterial elastance (E_a), respectively. LV contractility, loading conditions, and heart rate were varied over wide ranges, and a total of 76 data sets were obtained for S_m (1.2–9.1 cm/sec), E_{es}' (1.5–17.6 mm Hg/mL), V_{ed} (11–99 mL), E_a (3.6–58.4 mm Hg/mL), EJT (100–246 msec), heart rate (66–192 beats/min), and the ventricular-arterial coupling ratio (E_{es}'/E_a ; 0.2–3.0).

Results: The theoretical model accurately predicted S_m ($R^2 = 0.79$, $P < .0001$). By univariate analysis, S_m was correlated significantly with E_{es}' ($R^2 = 0.64$, $P < .0001$) and with the reciprocal of E_a ($R^2 = 0.49$, $P < .01$). V_{ed} and EJT did not affect S_m . E_{es}'/E_a was correlated strongly with S_m ($R^2 = 0.73$, $P < .0001$). E_{es}' and the reciprocal of E_a were not correlated with each other.

Conclusions: LV contractility and afterload independently determine S_m . The effects of LV preload and EJT on S_m might be small, even though they are theoretically associated with S_m . S_m strongly reflects the status of ventricular-arterial coupling. (J Am Soc Echocardiogr 2011;24:582-91.)

Keywords: Echocardiography, Heart failure, Hemodynamics, Mechanics

Left ventricular (LV) longitudinal shortening during ejection is reflected by systolic mitral annular velocity, which can be measured by tissue Doppler (TD) echocardiography in clinical practice.¹ Peak systolic mitral annular velocity (S_m) has been reported to be an index of global LV systolic function.^{2,3} Measurement of S_m allows the detection of cardiac dysfunction more sensitively than the evaluation of other conventional LV function indexes, such as LV ejection fraction (LVEF).⁴ S_m is a powerful prognosticator of mortality in patients with heart failure⁵ and in the general population.⁶

From the Department of Cardiovascular Dynamics, National Cerebral and Cardiovascular Center Research Institute, Suita, Japan (K.U., T.K., M.S.); and the Department of Cardiovascular Medicine, Kyushu University Graduate School of Medical Sciences, Fukuoka, Japan (K.S.).

This work was supported by a grant-in-aid for scientific research (C-20500404) from the Ministry of Education, Culture, Sports, Science and Technology and by the Intramural Research Fund (22-1-5) for Cardiovascular Diseases of the National Cerebral and Cardiovascular Center.

Reprint requests: Kazunori Uemura, MD, PhD, Department of Cardiovascular Dynamics, National Cerebral and Cardiovascular Center Research Institute, 5-7-1 Fujishirodai, Suita 565-8565, Japan (E-mail: kuemura@ri.ncvc.go.jp).

0894-7317/\$36.00

Copyright 2011 by the American Society of Echocardiography.

doi:10.1016/j.echo.2011.01.010

582

Although these previous studies have highlighted the clinical utility of S_m measurement, the mechanical determinants of S_m remain poorly defined.

S_m is correlated positively with LVEF in patients with cardiac diseases.² A recent animal study demonstrated that S_m is correlated with the maximum value of the time derivative of LV pressure (LVP) (LV dP/dt_{max}), an indicator of LV systolic function.⁷ These findings suggest that LV contractility contributes significantly to S_m . However, the magnitudes of LVEF and dP/dt_{max} change in response to alteration in loading conditions, even if the intrinsic LV contractility is preserved.⁸ Intriguingly, S_m and LV end-systolic elastance (E_{es} ; a relatively load independent index of LV contractility) were found not to be correlated in patients with hypertension.⁹ Henein *et al.*¹⁰ assessed the effects of acute alterations in afterload on S_m during peripheral vascular surgery and reported that an increase in afterload by aortoiliac clamping decreased S_m . In contrast, in patients undergoing cardiac surgery, S_m was insensitive to changes in afterload after infusions of vasoactive agents.¹¹

Whether and to what degree LV contractility and loading conditions independently affect S_m remain controversial. A more comprehensive approach is required to address this issue. The purpose of this study was to clarify the mechanisms that regulate the magnitude of S_m . To that end, we first derived the theoretical relationship between S_m and cardiovascular parameters describing LV contractility,

Abbreviations	
CV	= Coefficient of variation
E_a	= Effective arterial elastance
E_{es}	= End-systolic elastance
EJT	= Ejection time
HR	= Heart rate
LV	= Left ventricular
LVEF	= Left ventricular ejection fraction
LVP	= Left ventricular pressure
LVV	= Left ventricular volume
P_{es}	= End-systolic pressure
S_m	= Peak systolic mitral annular velocity
S_{mTD}	= Peak systolic myocardial velocity on tissue Doppler echocardiography
SV	= Stroke volume
SVR	= Systemic vascular resistance
TD	= Tissue Doppler
V_{ed}	= End-diastolic volume
V_{es}	= End-systolic volume

afterload, and preload. Second, in canine experiments, we simultaneously acquired LVP, LV volume (LVV), and S_m using a catheter-tipped micromanometer and sonomicrometer, while varying LV contractility and loading conditions over wide ranges. We compared these experimental data with the theoretical predictions and evaluated the independent effects of the parameters on S_m.

METHODS

Theoretical Relationship Between S_m and Cardiovascular Parameters

We based our theoretical modeling on the LVP-LVV framework,¹² as shown in Figure 1. E_{es}, the slope of the relationship between end-systolic pressure (P_{es}) and end-systolic volume (V_{es}), is an index of LV contractility (Figure 1A). Effective arterial elastance, E_a, the slope of the relationship between P_{es} and stroke volume (SV), is an index of LV afterload.¹³ The time-elastance curve of the left ventricle

has a distinct waveform (Figure 1B).^{14,15} The time-elastance curve during systole can be approximated to two straight lines, one for the isovolumic contraction phase and the other for the ejection phase (Figure 1B).^{14,15} S_m is related to E_{es}, E_a, LV end-diastolic volume (V_{ed}) and ejection time (EJT) by the following formula:

$$S_m = \frac{\alpha}{3} \cdot \frac{E_{es}}{E_a} \cdot \frac{V_{ed}^{1/3}}{EJT} \quad (1)$$

where α is a constant determined by the ratio of LV longitudinal to short-axis length. Details of the mathematical derivation of equation 1 are provided in the Appendix.

Animal Experiments

We used 22 adult mongrel dogs (both sexes; weight, 20–30 kg). The investigation conformed with the *Guide for the Care and Use of Laboratory Animals*.¹⁶ All protocols were approved by the Animal Subjects Committee of the National Cerebral and Cardiovascular Center.

Experiment 1: Comparison of Mitral Annular Velocities Measured by Sonomicrometry and TD Echocardiography

Preparation. Six animals were used. After anesthesia was induced with sodium pentobarbital (25 mg/kg), the animals were intubated endotracheally and ventilated artificially. An appropriate level of anesthesia was maintained by continuous inhalation of 1.5% isoflurane.

A sterile left lateral thoracotomy was performed, and the pericardium was opened. Three spheric sonomicrometer crystals (2 mm in diameter) were implanted in the subepicardium at the base (Figure 2A, points 1 and 2) and apex (Figure 2A, point 3) of the left ventricle. All wires were exteriorized through the back of the neck. The pericardium and chest wall were closed, and the animal was allowed to recover.

After the animals had fully recovered from the procedure (10–14 days after surgery), mitral annular velocities were measured by sonomicrometry and TD echocardiography. During measurements, the dogs were anesthetized and artificially ventilated and were laid in a sling. Surface electrocardiograms were recorded.

Mitral Annular Velocity Measurement by Sonomicrometry. To obtain LV dimensions, sonomicrometric signals were processed with a digital system (Sonolab, Sonometrics Corporation, London, Canada) while each crystal sent a signal to and received a signal from each of the other crystals. Analog signals of sonomicrometric LV dimensions and electrocardiography were digitized at 200 Hz and stored for offline analysis (Sonolab). The dimensions of the three sonomicrometer crystals were used to calculate the LV longitudinal length (L), which is the distance between the LV apex and the center of the base (Figure 2A). The time derivative of L (dL/dt) was used as instantaneous mitral annular velocity, and a positive velocity was reported to indicate shortening of L.¹⁷ Peak dL/dt during LV systole was used as S_m.

Mitral Annular Velocity Measurement by TD Echocardiography. Transthoracic echocardiography was performed using an echocardiographic system equipped with a 6-MHz transducer (Artida; Toshiba Corporation, Tokyo, Japan). Mitral annular velocity was obtained with pulsed TD from the apical four-chamber view by placing a 2-mm-wide sample volume at the septal side of the mitral annulus (Figure 2B).³ Peak systolic myocardial velocity (S_{mTD}) was obtained.^{3,5}

Data Acquisition. All data were acquired at end-expiration. To avoid interference between sonomicrometry and TD echocardiography, we first recorded echocardiographic data for 10 sec and then sonomicrometric dimensions during the subsequent 10 sec. Doses of dobutamine (2, 4, 8, and 16 μ g/kg/min) and propranolol (0.2 mg/kg) were administered intravenously to each dog to modulate LV inotropy. S_m and S_{mTD} were determined after administration of each dose.

Experiment 2: Effects of Cardiovascular Parameters on S_m

Preparation. Sixteen animals were used. Anesthesia and artificial ventilation were conducted as described above. A fluid-filled catheter (8Fr) was placed in the right femoral artery to measure systemic arterial pressure. The fluid-filled catheter was connected to a pressure transducer (DX-200; Nihon Kohden, Tokyo, Japan). After a median sternotomy, the heart was suspended in a pericardial cradle. A pair of pacing electrodes was fixed at the right atrial appendage for atrial pacing. A catheter-tipped micromanometer (PC-751; Millar Instruments, Houston, TX) was inserted via the LV apex to measure LVP. As depicted in Figure 3A, 10 sonomicrometer crystals were implanted in the subepicardium of the left ventricle and the right side of the interventricular septum to obtain LV dimensions. Surface electrocardiograms were recorded. After the instrumentation was completed, the pericardium was closed. All data acquisitions were done at end-expiration. Analog signals of arterial pressure, LVP,

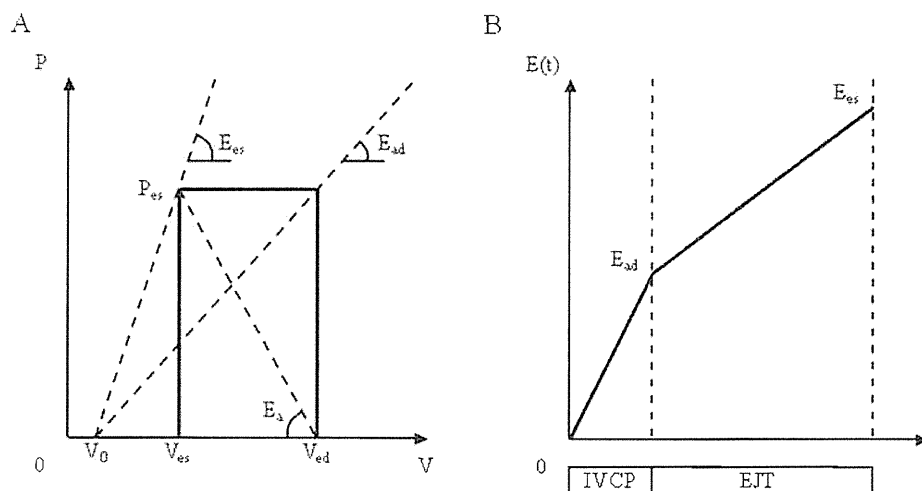


Figure 1 (A) Schematic drawing of the LVP (P)–LVV (V) loop, depicting E_{es} , E_{ad} , E_a , P_{es} , volume axis intercept of the relationship between P_{es} and V_{es} (V_0), V_{es} , and V_{ed} . (B) Bilinearly approximated time (t)–elastance ($E(t)$) curve during the isovolumic contraction phase (IVCP) and EJT.

sonomicrometric LV dimensions, and electrocardiography were digitized at 200 Hz and stored for offline analysis.

Experimental Protocols. After the initial preparation and surgical procedures were complete, the animals were allowed to stabilize for 30 min. Under steady-state baseline condition, we recorded the analog signals for about 10 sec in each animal. After obtaining the hemodynamic data at baseline conditions, we created various hemodynamic conditions, as described in the following protocols. In each protocol, we waited 20 min to confirm that hemodynamic conditions reached steady state.

Contractility Run (n = 9).—Hemodynamic data were recorded while LV contractility was increased by dobutamine infusion ($5 \mu\text{g}/\text{kg}/\text{min}$). After the data were recorded, dobutamine infusion was temporarily suspended. We created acute heart failure by embolizing the left coronary artery with glass microspheres ($90 \mu\text{m}$ in diameter). Data recording was repeated under depressed LV contractility. Hemodynamic data were also recorded after LV contractility was restored by reinfusion of dobutamine.

Loading Run (n = 7).—Hemodynamic data were recorded after pharmacologically altering vascular resistance (afterload) and LV filling (preload) by infusing norepinephrine ($0.2 \mu\text{g}/\text{kg}/\text{min}$), sodium nitroprusside ($3 \mu\text{g}/\text{kg}/\text{min}$), or 250 mL of 10% dextran 40.

Heart Rate (HR) Run (n = 6).—The possible dependence of S_m on HR was tested by suppressing the intrinsic atrial beat using zatebradine (UL-FS49; $0.5 \text{ mg}/\text{kg}$) and instituting atrial pacing to obtain hemodynamic data at different HRs ($\pm 25\%$ of baseline HR).

Six animals underwent both loading and HR runs. At the conclusion of the experiments, the dogs were sacrificed with an intravenous injection of pentobarbital and potassium chloride. Autopsies were performed to verify the position of the sonomicrometer crystals and catheters. After excision of the adjacent right ventricular muscle, valvular tissue and fat, LV myocardial volume was measured by water displacement in a volumetric cylinder.

Data Analysis and Definitions. Calculation of S_m .—Dimensions between the sonomicrometer crystals placed at the LV base (Figure 3A, points 1 and 2) and the LV apex (Figure 3A, point 3) were used to calculate S_m , as described above.

LVV Calculation Using Sonomicrometric LV Dimensions.—The three-dimensional position of each crystal was defined as a function of time on the basis of the distances between the crystals.¹⁸ The LV epicardial volume (including LVV and LV myocardial volume) was estimated using software that applied an ellipsoidal shell model to the coordinates of all 10 crystals (Figure 3A).¹⁹ LVV was obtained by subtracting LV myocardial volume from the estimated LV epicardial volume. Our preliminary study demonstrated that ex vivo LVV thus estimated agreed reasonably well with the volume measured by intraventricular balloon method (LVV_{ba}) in four canine hearts ($\text{LVV} = 1.0 \times \text{LVV}_{ba} - 7.0$; $r = 0.98$; $\text{SEE} = 14 \text{ mL}$; $20 \leq \text{LVV}_{ba} \leq 70 \text{ mL}$).

Cardiovascular Parameters.—End-systole was defined as the time when LV dP/dt decreased to 20% of its minimum.¹⁵ LV contractility was indexed by the P_{es}/V_{es} ratio ($E_{es}' = P_{es}/V_{es}$), which is an approximation of E_{es} .^{9,20} V_{ed} (an index of LV preload) was defined as LVV at the peak of the R wave on the electrocardiogram.¹¹ E_a (an index of LV afterload) was defined as the ratio of P_{es} to SV ($\text{SV} = V_{ed} - V_{es}$).^{9,13} The end of the isovolumic contraction phase was defined as the moment when LV dP/dt decreased to 80% of its maximum, according to a previous study²¹ with minor modification. EJT was obtained by subtracting the end of the isovolumic contraction phase from end-systole. Systemic vascular resistance (SVR) was defined as time-averaged arterial pressure divided by the product of SV and HR. A previous study demonstrated that E_a is related to SVR and HR as follows: $E_a \approx k \times \text{SVR} \times \text{HR}$, where k is a constant.¹³ The E_{es}'/E_a ratio was used as an index of ventricular-arterial coupling.^{14,20}

S_m and cardiovascular parameters were the averages of approximately 10 beats.

Statistical Analysis

All data are presented as mean \pm SD. Statistical analyses were performed using commercially available software (Statistica; Statsoft, Inc., Tulsa, OK). In experiments 1 and 2, the associations among variables were analyzed using a mixed-model procedure to handle the dependencies in repeated measurements within the same animal.^{7,17,22,23} The coefficient of determination (R^2) was used to evaluate the strength of association, because it measures how much variability of the dependent variable is the result of the independent

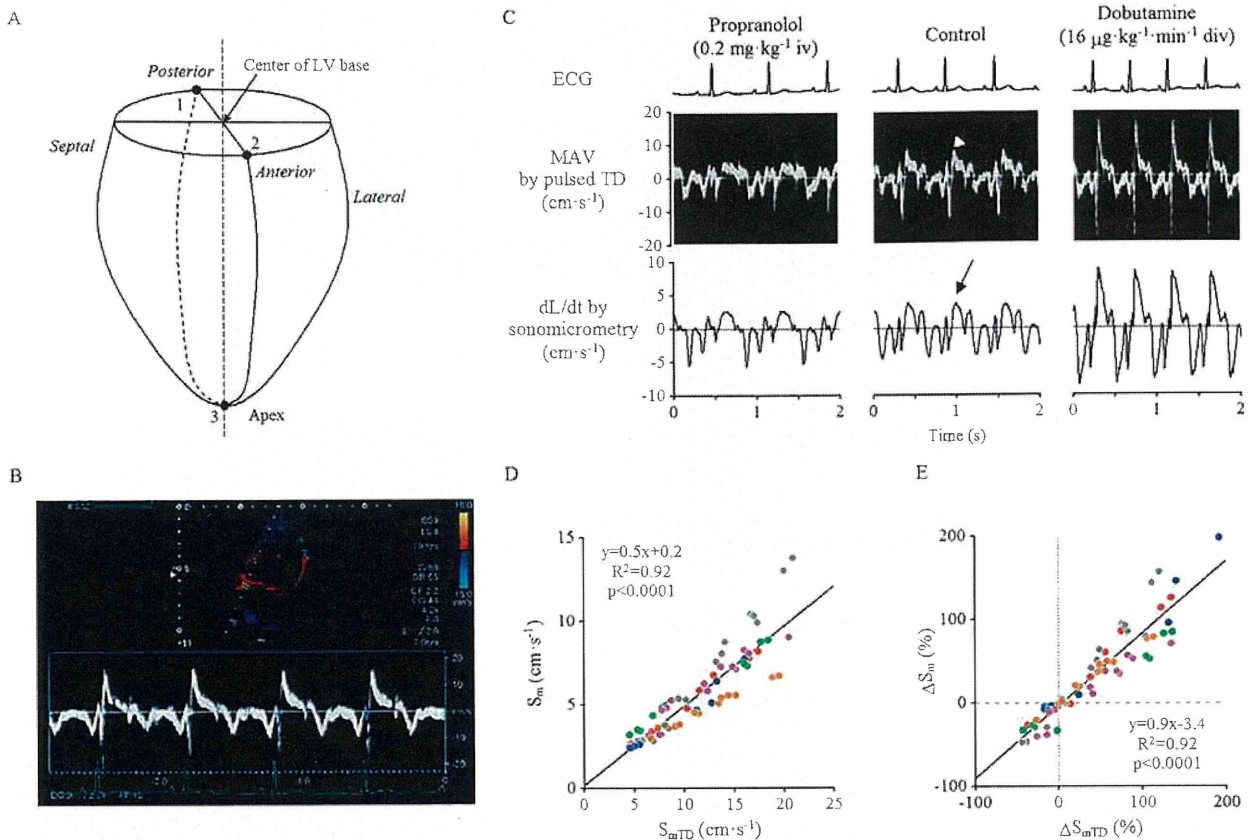


Figure 2 (A) Placement of sonomicrometer crystals (see text) in experiment 1. (B) Measurement of mitral annular velocity (MAV) at the septal side of the mitral annulus by TD echocardiography. (C) Examples of waveform data of electrocardiogram, septal MAV obtained from TD echocardiography, and dL/dt measured by implanted sonomicrometer crystals during hemodynamic alterations induced by dobutamine and propranolol. Data for dL/dt were traced so that positive values indicated shortening of LV longitudinal length.¹⁷ Because of interference between sonomicrometry and Doppler, TD velocities were not from the same heartbeat as the other recordings. Arrowhead, S_{mTD} ; arrow, S_m . (D) Relation between S_m and S_{mTD} in six dogs. Each color indicates the data from one animal. The line represents the population-averaged regression²⁰ between S_m and S_{mTD} with regression equation, coefficient of determination (R^2), and probability value. (E) Relation between percentage changes in S_m (ΔS_m) and S_{mTD} (ΔS_{mTD}) from their respective baseline values in six dogs. Each color indicates the data from one animal. The line represents the population-averaged regression between ΔS_m and ΔS_{mTD} with regression equation, R^2 , and probability value.

variable.⁷ In experiment 2, the coefficient of variation (CV) was calculated as the ratio of the SD to the mean (reported as a percentage) and used to quantify the variability of measurements. One-way repeated-measures analyses of variance with Dunnett's test were used in multiple comparisons relative to baseline for each intervention. P values < .05 were considered statistically significant.

RESULTS

Experiment 1: Mitral Annular Velocity Measured by Sonomicrometry and TD Echocardiography

Figure 2C displays representative recordings of mitral annular velocity measured by TD echocardiography and dL/dt measured by sonomicrometry when LV contractility was pharmacologically modulated. Waveforms derived from TD echocardiography were slightly different from those derived from sonomicrometry. As shown in Figure 2D, the values of S_{mTD} were consistently larger than those of S_m , but the two were correlated strongly on the basis of the data obtained from six canine hearts over a wide range of LV inotropy ($R^2 = 0.92$). Percentage change in S_{mTD} was also correlated highly with

percentage change in S_m ($R^2 = 0.92$; Figure 2E). On the basis of these findings, instead of S_{mTD} , we used S_m by sonomicrometry to investigate the mechanical determinants of systolic mitral annular velocity, because this allowed analyses of all variables, including LVP and LVV, from the same heartbeat.

Experiment 2: Effects of Cardiovascular Parameters on S_m

Figure 3B shows traces of hemodynamic variables in one animal under baseline conditions. As predicted in our theoretical analysis (Appendix), S_m was detected early in the ejection phase.

Effects of Various Interventions on S_m and Cardiovascular Parameters

Table 1 summarizes the effects of various interventions on S_m and cardiovascular parameters (a total of 76 data sets). The CVs for S_m , $E_{es'}$, V_{cd} , E_a , EJT, SVR, HR, and $E_{es'}/E_a$ were 44%, 49%, 41%, 77%, 24%, 77%, 21%, and 64%, respectively. S_m and all the cardiovascular parameters changed over reasonably wide ranges by the interventions.

Contractility Run.— S_m , $E_{es'}$, and $E_{es'}/E_a$ changed in a similar pattern from their respective baseline values. They increased significantly with

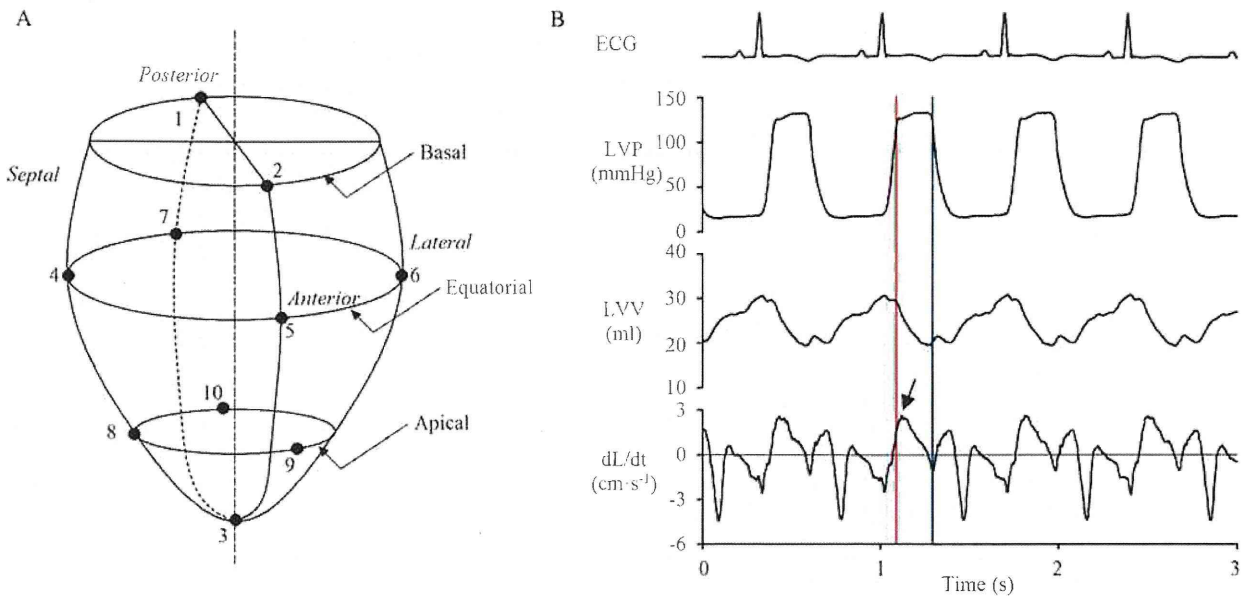


Figure 3 (A) Placement of sonomicrometer crystals (see text) in experiment 2. (B) Representative tracings from a dog in baseline condition. Vertical red line, end of isovolumic contraction phase; vertical blue line, end-systole; arrow, S_m .

dobutamine infusion, decreased significantly after acute heart failure induction, and recovered to baseline levels with reinfusion of dobutamine. V_{ed} and E_a significantly increased and EJT significantly decreased from their respective baseline values after acute heart failure induction.

Loading Run.— S_m , E_{es}' , and E_{es}'/E_a did not change significantly in response to changes in loading conditions. Norepinephrine infusion significantly increased E_a and SVR and significantly decreased HR. Sodium nitroprusside infusion significantly decreased V_{ed} but did not significantly reduce E_a and SVR. Dextran infusion significantly increased V_{ed} and EJT and significantly decreased E_a and HR.

HR Run.—Zatebradine infusion significantly decreased HR and E_{es}' and significantly increased V_{ed} and EJT. Atrial tachypacing significantly increased HR. E_a was apparently decreased by zatebradine and increased by atrial tachypacing, although the differences were not significant.

Relationships Between S_m and Cardiovascular Parameters. Using the 76 data sets from all interventions, we examined whether S_m was related to the cardiovascular parameters as predicted by equation 1. As shown in Figure 4A, S_m was correlated significantly with the product of E_{es}' and the cubic root of V_{ed} divided by E_a and EJT. The R^2 value was 0.79, indicating that the theoretical model accurately predicts S_m .

Figures 4B to 4H shows univariate relationships between S_m and each of the cardiovascular parameters. S_m was correlated significantly with E_{es}' (Figure 4B). In accordance with equation 1, we related S_m with the cubic root of V_{ed} ($V_{ed}^{1/3}$; Figure 4C), with the reciprocal of E_a (E_a^{-1} ; Figure 4D), and with the reciprocal of EJT (EJT^{-1} ; Figure 4E). The CVs for E_a^{-1} , $V_{ed}^{1/3}$, and EJT^{-1} were 41%, 14%, and 21%, respectively. S_m was correlated significantly with E_a^{-1} but not with $V_{ed}^{1/3}$ and EJT^{-1} . Because E_a was correlated linearly with the product of SVR and HR, as described above, we related S_m with the reciprocal of SVR (SVR^{-1} ; Figure 4F) and with the reciprocal of HR (HR^{-1} ; Figure 4G). S_m was correlated significantly with SVR^{-1}

but not with HR^{-1} . Figure 4H indicates that E_{es}'/E_a was tightly correlated with S_m .

We analyzed the correlations between the cardiovascular parameters. E_{es}' was not correlated with E_a^{-1} ($P = .96$), indicating that the two affect S_m independently. E_{es}' was correlated inversely with $V_{ed}^{1/3}$ ($E_{es}' = -4.3 \times V_{ed}^{1/3} + 21.7$; $R^2 = 0.56$, $P < .001$). E_a^{-1} was correlated inversely with EJT^{-1} ($E_a^{-1} = -0.03 \times EJT^{-1} + 0.34$; $R^2 = 0.76$, $P < .0001$). E_a^{-1} was correlated positively with $V_{ed}^{1/3}$ ($E_a^{-1} = 0.05 \times V_{ed}^{1/3} + 0.03$; $R^2 = 0.68$, $P < .01$). $V_{ed}^{1/3}$ was correlated inversely with EJT^{-1} ($V_{ed}^{1/3} = -0.16 \times EJT^{-1} + 4.45$; $R^2 = 0.76$, $P < .001$).

DISCUSSION

To the best of our knowledge, this is the first study to comprehensively evaluate the relations between S_m and cardiovascular parameters using theoretical modeling and also well-controlled animal experiments. The theoretical model of S_m indicates that S_m is affected by LV contractility, preload, afterload, and EJT. Experimental data confirmed that the theoretical model accurately predicts S_m . Further analysis of the experimental data showed that LV contractility and afterload have independent effects on S_m , but LV preload and EJT do not. S_m strongly reflects the status of ventricular-arterial coupling.

Mechanical Determinants of S_m

The theoretical model of S_m is rational mechanically because the right side of equation 1 corresponds to the mean velocity of LV shortening. The product of E_{es}'/E_a and V_{ed} positively correlates with SV.¹³ Therefore, the product of E_{es}'/E_a and the cubic root of V_{ed} , which corresponds to LV end-diastolic dimension, positively correlates with the stroke dimension of the left ventricle. The stroke dimension of the left ventricle divided by EJT equals the mean velocity of LV shortening.

In our theoretical analysis, we assumed that changes in LV length couple with changes in LVV (Appendix). Actually, this is not the case throughout the cardiac cycle. In the isovolumic contraction

Table 1 Effect of interventions on systolic mitral annular velocity and cardiovascular parameters

Variable	S_m (cm/sec) 3.3 ± 1.5 (1.2–9.1)	E_{es}' (mm Hg/mL) 7.5 ± 3.7 (1.5–17.6)	V_{ed} (mL) 37 ± 16 (11–99)	E_a (mm Hg/mL) 9.2 ± 7.1 (3.6–58.4)	EJT (msec) 150 ± 36 (100–246)	SVR (mm Hg/sec/mL) 4.4 ± 3.3 (1.3–21.4)	HR (beats/min) 130 ± 28 (66–192)	E_{es}'/E_a 1.0 ± 0.7 (0.2–3.0)	<i>n</i> 76
Contractility run									
Baseline	3.4 ± 1.2	6.2 ± 1.7	38 ± 9	6.7 ± 1.4	134 ± 12	2.9 ± 0.7	130 ± 11	1.0 ± 0.4	9
DOB	6.0 ± 1.8 [†]	10.5 ± 3.7 [†]	45 ± 5	6.1 ± 1.6	127 ± 8	2.7 ± 1.1	136 ± 24	1.9 ± 0.9 [†]	9
AHF	2.2 ± 1.0*	2.7 ± 0.8 [†]	50 ± 17 [†]	8.4 ± 2.4*	121 ± 13 [†]	3.2 ± 1.0	145 ± 12	0.3 ± 0.1*	9
AHF with DOB	3.5 ± 0.9	4.3 ± 1.4	56 ± 17 [†]	7.4 ± 1.3	117 ± 6 [†]	2.8 ± 0.8	156 ± 26 [†]	0.6 ± 0.1	9
Loading run									
Baseline	2.9 ± 0.7	9.3 ± 3.2	24 ± 7	10.6 ± 4.5	161 ± 21	5.2 ± 2.4	127 ± 19	1.1 ± 0.7	7
NE	2.8 ± 0.6	10.9 ± 3.9	29 ± 9	14.8 ± 7.9 [†]	165 ± 25	9.0 ± 5.4 [†]	103 ± 24 [†]	0.9 ± 0.4	7
SNP	3.1 ± 0.6	9.5 ± 3.6	19 ± 6*	9.1 ± 4.3	158 ± 31	4.6 ± 2.0	127 ± 17	1.3 ± 0.8	7
DEX	3.1 ± 0.9	7.2 ± 1.6	39 ± 10 [†]	7.1 ± 3.5*	209 ± 26 [†]	3.9 ± 1.9	107 ± 14*	1.2 ± 0.5	7
Heart rate run									
Baseline	2.8 ± 0.7	9.9 ± 3.0	24 ± 7	10.5 ± 5.0	155 ± 16	4.8 ± 2.3	134 ± 8	1.1 ± 0.7	6
ZAT	2.9 ± 1.1	6.9 ± 1.0*	39 ± 9 [†]	6.6 ± 3.0	204 ± 33 [†]	4.5 ± 2.2	86 ± 4 [†]	1.2 ± 0.4	6
PACE	3.0 ± 1.4	10.0 ± 2.7	22 ± 9	18.4 ± 19.9	143 ± 22	6.9 ± 7.3	165 ± 12 [†]	0.9 ± 0.4	6

Data are shown as mean ± SD (range). Because there was an overlap in baseline parameters between the loading and heart rate runs, the sum of the numbers of all interventions was not 82, but 76.

AHF, Acute heart failure induced by coronary embolization; DEX, dextran infusion; DOB, dobutamine infusion; NE, norepinephrine infusion; PACE, atrial tachypacing; SNP, sodium nitroprusside infusion; ZAT, zatebradine infusion.

**P* < .05.

[†]*P* < .01 versus baseline.

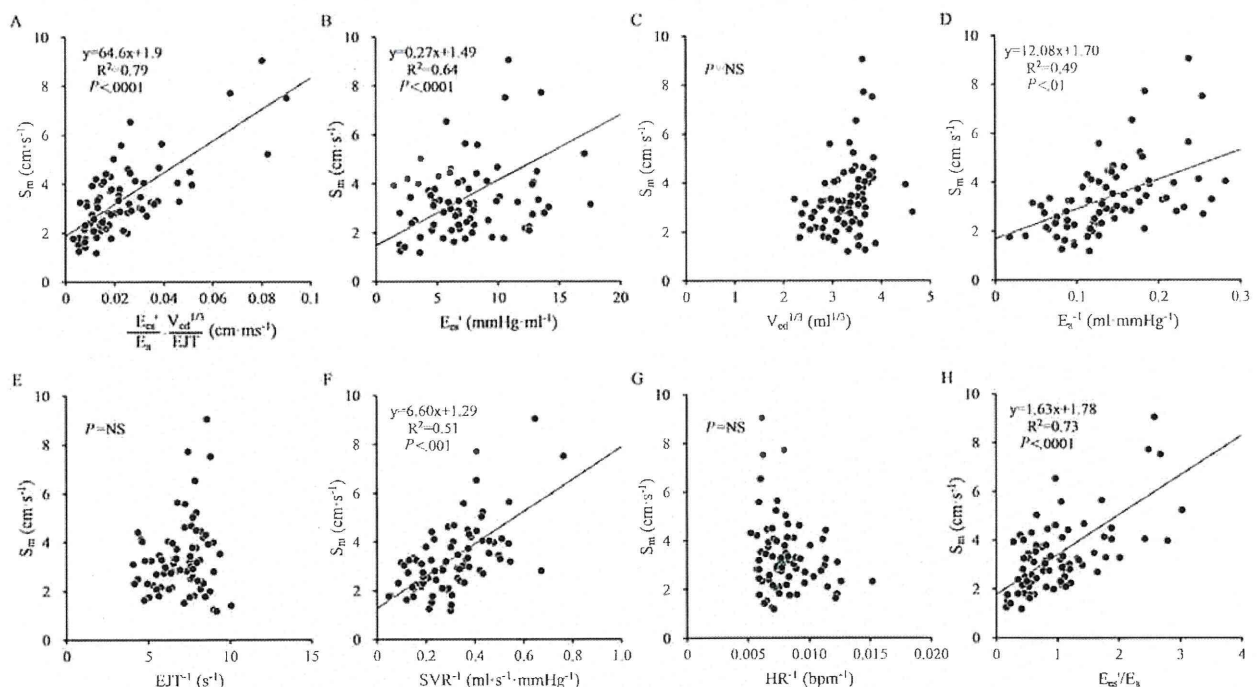


Figure 4 (A) Relationship between measured S_m and values obtained from the theoretical model consisting of the ratio of P_{es} to V_{es} (E_{es}'), V_{ed} , E_a , and EJT (see equation 1). (B–H) Relationships between S_m and E_{es}' (B), the cubic root of V_{ed} (C), the reciprocal of E_a (D), the reciprocal of EJT (E), the reciprocal of SVR (F), the reciprocal of HR (G), and the ventricular-arterial coupling ratio (E_{es}'/E_a) (H). Each panel shows raw data from all interventions (76 data points) and the line representing the population-averaged regression between S_m and the cardiovascular parameters,²⁰ regression equation, R^2 , and probability value.

phase, LV longitudinal and short-axis lengths change without change in LVV.¹⁹ However, during the ejection phase, which was the phase of interest in our analysis, both LV longitudinal and short-axis lengths de-

creased in parallel with LVV. We also assumed that the ratio of LV longitudinal length to short-axis length is constant during the ejection phase (Appendix). The ratio is actually not constant. The ratio

averaged for eight dogs in a previous study was 1.65 at the beginning of the ejection phase.¹⁹ At the end of the ejection phase, the ratio increased to 1.88. If these values are translated into α in equation 1, α increases from 1.73 to 1.89 (a net increase of 10%) during the ejection phase. Hence, α is actually not constant within one animal. Although this can be a confounder in this theoretical analysis (Appendix), its effect would be quantitatively small. Apart from α , the time-varying LV elastance, $E(t)$, also determines S_m (equation A9 in Appendix). If $E(t)$ is constant, S_m is achieved when α is maximum, that is, at the end of the ejection phase. Meanwhile, if α is constant, S_m is achieved when $E(t)$ is minimum, that is, at the beginning of the ejection phase. During the ejection phase, $E(t)$ increases from 5 to 10 mm Hg/mL in dogs (a net increase of 100%).¹⁵ A numerical simulation using these published data indicates that the contribution of $E(t)$ to S_m is 15 times more than that of α . Thus, we can assume α as constant without sacrificing accuracy. S_m is effectively determined by $E(t)$ and is achieved at the beginning of the ejection phase. This is compatible with in vivo findings. In this study (Figures 2B, 2C, and 3B) and also in previous studies,^{4,7,23} S_m is usually reached early in the ejection phase.

According to the value of R^2 , the theoretical model can predict 79% of S_m variation. The residual variation, 21%, remains to be explained. Although it is possible that variation among animals of α in equation 1 may contribute to this residual variation, the CV of α in eight dogs was <5% in a previous study,¹⁹ suggesting that variation among animals of α plays a minor role in the residual variation. The variation may be caused by factors not included in the model. A previous study indicated that dynamic arterial properties such as aortic compliance have direct effects on S_m .¹⁰ Further studies to address these issues are required in the future.

LV contractility determines the magnitude of S_m . The R^2 value of 0.64 between S_m and E_{es}' in this study was comparable with those observed between S_m and other LV functional indexes, such as LV dP/dt_{max} , in previous studies.⁷ Borlaug *et al.*⁹ reported that S_m was not correlated with indexes of LV contractility including, E_{es}' , in patients with hypertension. However, because they excluded patients with heart failure with depressed LV contractility from the study population and did not actively stimulate LV inotropy in their protocol, LV contractile indexes were well preserved with small variations among patients. This might be a reason they did not detect a significant correlation between S_m and indexes of LV contractility.

S_m is inversely related to LV afterload. Previous clinical studies have yielded contrasting results of dependence^{9,10,24} and independence^{11,25} of S_m on afterload. Oki *et al.*²⁴ reported that S_m was reduced in response to an increase in LV afterload after angiotensin infusion in healthy subjects. In contrast, Amà *et al.*¹¹ reported that S_m did not change when E_a and SVR were changed by phenylephrine or nitroglycerine infusion in patients undergoing cardiac surgery. However, they did not attempt to directly associate S_m with the afterload indexes. Similar to their results, we also noted that S_m did not change in response to phenylephrine infusion, whereas E_a or SVR significantly increased (Table 1). However, we further analyzed the associations between S_m and afterload indexes using mixed-model procedures. In the previous studies, conducting statistical analyses similar to those we performed in this study would have been useful to evaluate association between the afterload and S_m .

Unexpectedly, V_{ed} and EJT did not affect S_m independently. Both V_{ed} and EJT are components of our theoretical model of S_m . Furthermore, previous studies suggested that S_m was affected by LV preload and EJT.^{23,26} In this study, the CVs for $V_{ed}^{1/3}$ and EJT^{-1} were small compared with those for E_{es}' and E_a^{-1} . Moreover, E_{es}'

was correlated inversely with $V_{ed}^{1/3}$, and E_a^{-1} was correlated inversely with EJT^{-1} . These suggest that because of the low variability of $V_{ed}^{1/3}$ and EJT^{-1} and the antagonizing effects of the covariates (E_{es}' and E_a^{-1}), the analysis might fail to detect significant correlations of $V_{ed}^{1/3}$ and EJT^{-1} with S_m . However, V_{ed} also was not correlated with S_m in this study (data not shown), although the CVs for V_{ed} and E_{es}' were comparable (41% and 49%). It would be ideal to change V_{ed} or EJT individually while keeping all other parameters constant. Although impedance loading on ex vivo heart preparation would realize such protocols,⁸ this preparation is inappropriate for the study of LV longitudinal function, because it requires resection of the mitral valve and subvalvular apparatus (papillary muscles), which are critical components of longitudinal function.²⁷ Taken together, although we cannot completely exclude significant contributions of LV preload and EJT to S_m , their effects may be small and easily reversed by the effects of LV contractility and afterload, that is, effectively negligible compared with the status of ventricular-arterial coupling.

Potential Clinical Implications

A novel and important finding of this study is that S_m strongly reflects the status of ventricular-arterial coupling. Ventricular-arterial coupling is a central determinant of cardiovascular performance and cardiac energetics.^{13-15,28,29} Normally, the left ventricle and the arterial system are optimally coupled to produce maximal stroke work, when E_{es}/E_a is near unity. Maximal energetic efficiency occurs when E_{es}/E_a approximates 2.0. In patients with heart failure, the left ventricle and the arterial system are suboptimally coupled (E_{es}/E_a becomes less than unity). Beta-blockade improves this situation.²⁰ In patients with myocardial infarction, suboptimal coupling ratio is associated with poor prognosis over the next 5 years.²⁹ S_m as a measure of the status of ventricular-arterial coupling may allow accurate evaluations of cardiovascular pathophysiology and also predictions of prognosis in patients with cardiac disease. The ventricular-arterial coupling ratio can be predicted also by LVEF.⁸ However, LVEF assessment requires precise definition of the endocardial borders on conventional echocardiography, which is complicated by trabeculae or endocardial dropout. Precise endocardial definition is sometimes difficult, especially in obese patients, the elderly, and patients with pulmonary disease. Recording of mitral annular motion has the advantage that it is not dependent on the endocardial definition and is therefore relatively independent of image quality.⁷ S_m measurement can be an alternative to LVEF assessment to predict the status of ventricular-arterial coupling in such patients.

Study Limitations

In accordance with a previous canine study,¹⁷ sonomicrometry consistently underestimated systolic mitral annular velocity compared with TD echocardiography (Figure 2D). This discrepancy may be attributed to the location of the crystals, which are implanted in the subepicardium. Although longitudinally directed myocardial fibers in both subendocardial and subepicardial layers of the left ventricle may play a major role in the magnitude of systolic mitral annular velocity,¹ systolic shortening of subepicardial fiber is significantly smaller than that of subendocardial fiber.³⁰ In humans, the absolute value of mitral annular velocity measured by TD echocardiography agreed with that measured by cardiac magnetic resonance imaging, which is the widely accepted gold standard for the assessment of LVV and function.³¹ Although sonomicrometry is useful in animal experiments

for the assessment of heart motion, our data suggest that S_m obtained by sonomicrometry in this study might have underestimated the true LV longitudinal shortening velocity. However, a strong correlation was observed between S_m and S_{mTD} (Figure 2D). Percentage changes in S_m and S_{mTD} were also correlated tightly (Figure 2E), indicating that S_m sensitively tracked changes in S_{mTD} . Taken together, it is fair to say that conclusions provided by sonomicrometry in this study are comparable, at least qualitatively, with those obtained by TD echocardiography.

In analyzing the experimental data, we relied on E_{es}' (the P_{es}/V_{es} ratio) to quantify LV contractility, which can be evaluated more precisely by both the slope (E_{es}) and volume axis intercept (V_0) of the relationship between P_{es} and V_{es} (Figure 1A).¹² It was unclear how each contributed to the magnitude of S_m in this study. Despite these limitations, the P_{es}/V_{es} ratio as a single contractile index simplifies the statistical analysis of contractility.^{9,20}

Colinearity among the cardiovascular parameters as noted between E_{es}' and $V_{ed}^{1/3}$ might have affected the present results. The colinearity may be attributable to the nature of the protocols, such as heart failure induction, which depresses LV contractility and increases preload simultaneously. However, the protocols are analogous to commonly observed clinical setting or practice, that is, relevant to possible clinical application of the conclusions of this study.

CONCLUSIONS

LV contractility and afterload independently determine S_m . The effects of LV preload and EJT on S_m might be small, even though they are theoretically associated with S_m . S_m strongly reflects the status of ventricular-arterial coupling.

REFERENCES

1. Nikitin NP, Witte KK, Thackray SD, de Silva R, Clark AL, Cleland JG. Longitudinal ventricular function: normal values of atrioventricular annular and myocardial velocities measured with quantitative two-dimensional color Doppler tissue imaging. *J Am Soc Echocardiogr* 2003;16:906-21.
2. Gulati VK, Katz WE, Follansbee WP, Gorcsan J III. Mitral annular descent velocity by tissue Doppler echocardiography as an index of global left ventricular function. *Am J Cardiol* 1996;77:979-84.
3. Hori Y, Sato S, Hoshi F, Higuchi S. Assessment of longitudinal tissue Doppler imaging of the left ventricular septum and free wall as an indicator of left ventricular systolic function in dogs. *Am J Vet Res* 2007;68:1051-7.
4. Mogelvang R, Goetze JP, Pedersen SA, Olsen NT, Marott JL, Schnohr P, et al. Preclinical systolic and diastolic dysfunction assessed by tissue Doppler imaging is associated with elevated plasma pro-B-type natriuretic peptide concentrations. *J Card Fail* 2009;15:489-95.
5. Nikitin NP, Loh PH, Silva R, Ghosh J, Khaleva OY, Goode K, et al. Prognostic value of systolic mitral annular velocity measured with Doppler tissue imaging in patients with chronic heart failure caused by left ventricular systolic dysfunction. *Heart* 2006;92:775-9.
6. Mogelvang R, Sogaard P, Pedersen SA, Olsen NT, Marott JL, Schnohr P, et al. Cardiac dysfunction assessed by echocardiographic tissue Doppler imaging is an independent predictor of mortality in the general population. *Circulation* 2009;119:2679-85.
7. Seo JS, Kim DH, Kim WJ, Song JM, Kang DH, Song JK. Peak systolic velocity of mitral annular longitudinal movement measured by pulsed tissue Doppler imaging as an index of global left ventricular contractility. *Am J Physiol Heart Circ Physiol* 2010;298:H1608-15.
8. Kass DA, Maughan WL, Guo ZM, Kono A, Sunagawa K, Sagawa K. Comparative influence of load versus inotropic states on indexes of ventricular contractility: experimental and theoretical analysis based on pressure-volume relationships. *Circulation* 1987;76:1422-36.
9. Borlaug BA, Melenovsky V, Redfield MM, Kessler K, Chang HJ, Abraham TP, et al. Impact of arterial load and loading sequence on left ventricular tissue velocities in humans. *J Am Coll Cardiol* 2007;50:1570-7.
10. Henein MY, Das SK, O'Sullivan C, Kakkar VV, Gillbe CE, Gibson DG. Effect of acute alterations in afterload on left ventricular function in patients with combined coronary artery and peripheral vascular disease. *Heart* 1996;75:151-8.
11. Amà R, Segers P, Roossens C, Claessens T, Verdonck P, Poelaert J. The effects of load on systolic mitral annular velocity by tissue Doppler imaging. *Anesth Analg* 2004;99:332-8.
12. Burkhoff D, Mirsky I, Suga H. Assessment of systolic and diastolic ventricular properties via pressure-volume analysis: a guide for clinical, translational, and basic researchers. *Am J Physiol Heart Circ Physiol* 2005;289:H501-12.
13. Sunagawa K, Maughan WL, Burkhoff D, Sagawa K. Left ventricular interaction with arterial load studied in isolated canine ventricle. *Am J Physiol Heart Circ Physiol* 1983;245:H773-80.
14. Hayashi K, Shigemi K, Shishido T, Sugimachi M, Sunagawa K. Single-beat estimation of ventricular end-systolic elastance-effective arterial elastance as an index of ventricular mechanoenergetic performance. *Anesthesiology* 2000;92:1769-76.
15. Shishido T, Hayashi K, Shigemi K, Sato T, Sugimachi M, Sunagawa K. Single-beat estimation of end-systolic elastance using bilinearly approximated time-varying elastance curve. *Circulation* 2000;102:1983-9.
16. National Institutes of Health. Guide for the care and use of laboratory animals (NIH Publication No. 85-23). Bethesda, MD: National Institutes of Health; 1996.
17. Opdahl A, Remme EW, Helle-Valle T, Lyseggen E, Vartdal T, Pettersen E, et al. Determinants of left ventricular early-diastolic lengthening velocity: independent contributions from left ventricular relaxation, restoring forces, and lengthening load. *Circulation* 2009;119:2578-86.
18. Ratcliffe MB, Gupta KB, Streicher JT, Savage EB, Bogen DK, Edmunds LH Jr. Use of sonomicrometry and multidimensional scaling to determine the three dimensional coordinates of multiple cardiac locations: feasibility and initial implementation. *IEEE Trans Biomed Eng* 1995;42:587-98.
19. Rankin JS, McHale PA, Arentzen CE, Ling D, Greenfield JC Jr, Anderson RW. The three dimensional dynamic geometry of the left ventricle in the conscious dog. *Circ Res* 1976;39:304-13.
20. Maurer MS, Sackner-Bernstein JD, El-Khoury Rumbarger L, Yushak M, King DL, Burkhoff D. Mechanisms underlying improvements in ejection fraction with carvedilol in heart failure. *Circ Heart Fail* 2009;2:189-96.
21. Colin P, Ghaleb B, Monnet X, Hittinger L, Berdeaux A. Effect of graded heart rate reduction with ivabradine on myocardial oxygen consumption and diastolic time in exercising dogs. *J Pharmacol Exp Ther* 2004;308:236-40.
22. Fitzmaurice GM, Ravichandran C. A primer in longitudinal data analysis. *Circulation* 2008;118:2005-10.
23. Odland HH, Kro GA, Munkeby BH, Edvardsen T, Saugstad OD, Thaulow E. Ejection time-corrected systolic velocity improves accuracy in the evaluation of myocardial dysfunction: a study in piglets. *Pediatr Cardiol* 2010;31:1070-8.
24. Oki T, Fukuda K, Tabata T, Mishiro Y, Yamada H, Abe M, et al. Effect of an acute increase in afterload on left ventricular regional wall motion velocity in healthy subjects. *J Am Soc Echocardiogr* 1999;12:476-83.
25. Palmieri V, Russo C, Arezzi E, Pezzullo S, Sabatella M, Minichiello S, et al. Relations of longitudinal left ventricular systolic function to left ventricular mass, load, and Doppler stroke volume. *Eur J Echocardiogr* 2006;7:348-55.
26. Pelà G, Regolisti G, Coghi P, Cabassi A, Basile A, Cavatorta A, et al. Effects of the reduction of preload on left and right ventricular myocardial velocities analyzed by Doppler tissue echocardiography in healthy subjects. *Eur J Echocardiogr* 2004;5:262-71.

27. Jones CJ, Raposo L, Gibson DG. Functional importance of the long axis dynamics of the human left ventricle. *Br Heart J* 1990;63:215-20.
28. Burkhoff D, Sagawa K. Ventricular efficiency predicted by an analytical model. *Am J Physiol* 1986;250:R1021-7.
29. Antonini-Canterin F, Enache R, Popescu BA, Popescu AC, Ghingina C, Leiballi E, et al. Prognostic value of ventricular-arterial coupling and B-type natriuretic peptide in patients after myocardial infarction: a five-year follow-up study. *J Am Soc Echocardiogr* 2009;22:1239-45.
30. Sabbah HN, Marzilli M, Stein PD. The relative role of subendocardium and subepicardium in left ventricular mechanics. *Am J Physiol* 1981;240:H920-6.
31. Marsan NA, Westenberg JJ, Tops LF, Ypenburg C, Holman ER, Reiber JH, et al. Comparison between tissue Doppler imaging and velocity-encoded magnetic resonance imaging for measurement of myocardial velocities, assessment of left ventricular dyssynchrony, and estimation of left ventricular filling pressures in patients with ischemic cardiomyopathy. *Am J Cardiol* 2008;102:1366-72.

Did you know?

You can personalize the
JASE website to meet
your individual needs.

Visit www.onlinejase.com today!

APPENDIX

Instantaneous LVP, $P(t)$, and LVV, $V(t)$, are related by the following formula:

$$V(t) = \frac{P(t)}{E(t)} + V_0, \quad (\text{A2})$$

where $E(t)$ is time-varying LV elastance and V_0 is the volume axis intercept of the relationship between P_{es} and V_{es} .¹² S_m is a parameter of the ejection phase. The left ventricle has an ellipsoid shape, and the ratio of LV longitudinal length, $L(t)$, to short-axis length is assumed to be constant during the ejection phase. $L(t)$ and its time derivative are expressed as follows:

$$L(t) = \alpha[V(t)]^{1/3}, \quad (\text{A3})$$

$$dL(t)/dt = \frac{\alpha}{3} \cdot dV(t)/dt \cdot [V(t)]^{-2/3}. \quad (\text{A4})$$

During the ejection phase, because $P(t)$ can be approximated to P_{es} (Figure 1A), equation A2 is rewritten as follows:

$$V(t) = \frac{P_{es}}{E(t)} + V_0. \quad (\text{A5})$$

Differentiation of both sides of equation A5 with respect to time yields

$$dV(t)/dt = \frac{-P_{es} \cdot dE(t)/dt}{[E(t)]^2}. \quad (\text{A6})$$

During the ejection phase, because $E(t)$ increases linearly with respect to time,^{14,15} $dE(t)/dt$ is expressed as follows (Figure 1B):

$$dE(t)/dt = \frac{E_{es} - E_{ad}}{EJT}, \quad (\text{A7})$$

where E_{ad} is the elastance value at the end of the isovolumic contraction phase (Figure 1B).^{14,15} Substituting equation A7 into equation A6 yields

$$dV(t)/dt = \frac{-P_{es}}{[E(t)]^2 \cdot EJT} \cdot (E_{es} - E_{ad}). \quad (\text{A8})$$

Substituting equations A5 and A8 into equation A4 yields

$$dL(t)/dt = \frac{-\alpha}{3} \cdot \frac{P_{es}}{EJT} \cdot (E_{es} - E_{ad}) \cdot \frac{1}{[E(t)]^{4/3}} \cdot \left(\frac{1}{P_{es} + V_0 \cdot E(t)} \right)^{2/3}. \quad (\text{A9})$$

Peak shortening velocity of LV longitudinal length, S_m , corresponds to the absolute value of peak negative $dL(t)/dt$ during the ejection phase. Because $E(t)$ increases constantly during this period (Figure 1B), $dL(t)/dt$ assumes its peak negative value when $E(t)$ is E_{ad} . Hence, S_m can be expressed as follows:

$$S_m = \frac{\alpha}{3} \cdot \frac{P_{es}}{EJT} \cdot (E_{es} - E_{ad}) \cdot \frac{1}{E_{ad}^{4/3}} \cdot \left(\frac{1}{P_{es} + V_0 \cdot E_{ad}} \right)^{2/3}. \quad (\text{A10})$$

As shown in Figure 1A, E_{es} , E_{ad} , and E_a will be approximated by P_{es} , V_{es} , V_{ed} , and V_0 as follows:

$$E_{es} = \frac{P_{es}}{V_{es} - V_0}. \quad (\text{A11})$$

$$E_{ad} = \frac{P_{es}}{V_{ed} - V_0}. \quad (\text{A12})$$

$$E_a = \frac{P_{es}}{V_{ed} - V_{es}}. \quad (\text{A13})$$

Substituting V_{es} in equation A11 and V_{ed} in equation A12 into equation A13 yields

$$E_{es} - E_{ad} = \frac{E_{es} \cdot E_{ad}}{E_a}. \quad (\text{A14})$$

Substituting $(E_{es} - E_{ad})$ in equation A14 into equation A10 yields

$$S_m = \frac{\alpha}{3} \cdot \frac{P_{es}}{EJT} \cdot \frac{E_{es}}{E_a} \cdot \frac{1}{E_{ad}^{1/3}} \cdot \left(\frac{1}{P_{es} + V_0 \cdot E_{ad}} \right)^{2/3}. \quad (\text{A15})$$

Substituting E_{ad} in equation A12 into equation A15 yields

$$S_m = \frac{\alpha}{3} \cdot \frac{E_{es}}{E_a} \cdot \frac{V_{ed}^{1/3}}{EJT} \cdot \left(1 - \frac{V_0}{V_{ed}} \right). \quad (\text{A16})$$

If we assume that $V_{ed} \gg V_0$, equation A16 is rewritten as

$$S_m = \frac{\alpha}{3} \cdot \frac{E_{es}}{E_a} \cdot \frac{V_{ed}^{1/3}}{EJT},$$

which is equation 1 shown in the "Methods" section.



Medetomidine, an α_2 -Adrenergic Agonist, Activates Cardiac Vagal Nerve Through Modulation of Baroreflex Control

Shuji Shimizu, MD, PhD; Tsuyoshi Akiyama, MD, PhD; Toru Kawada, MD, PhD; Yusuke Sata, MD; Masaki Mizuno, PhD; Atsunori Kamiya, MD, PhD; Toshiaki Shishido, MD, PhD; Masashi Inagaki, MD; Mikiyasu Shirai, MD, PhD; Shunji Sano, MD, PhD; Masaru Sugimachi, MD, PhD

Background: Although α_2 -adrenergic agonists have been reported to induce a vagal-dominant condition through suppression of sympathetic nerve activity, there is little direct evidence that they directly increase cardiac vagal nerve activity. Using a cardiac microdialysis technique, we investigated the effects of medetomidine, an α_2 -adrenergic agonist, on norepinephrine (NE) and acetylcholine (ACh) release from cardiac nerve endings.

Methods and Results: A microdialysis probe was implanted into the right atrial wall near the sinoatrial node in anesthetized rabbits and perfused with Ringer's solution containing eserine. Dialysate NE and ACh concentrations were measured using high-performance liquid chromatography. Both 10 and 100 $\mu\text{g}/\text{kg}$ of intravenous medetomidine significantly decreased mean blood pressure (BP) and the dialysate NE concentration, but only 100 $\mu\text{g}/\text{kg}$ of medetomidine enhanced ACh release. Combined administration of medetomidine and phenylephrine maintained mean BP at baseline level, and augmented the medetomidine-induced ACh release. When we varied the mean BP using intravenous administration of phenylephrine, treatment with medetomidine significantly steepened the slope of the regression line between mean BP and log ACh concentration.

Conclusions: Medetomidine increased ACh release from cardiac vagal nerve endings and augmented baroreflex control of vagal nerve activity. (*Circ J* 2012; **76**: 152–159)

Key Words: Acetylcholine; Norepinephrine; Sinoatrial node; Sympathetic nervous system; Vagus nerve

The selective α_2 -adrenergic agonist, dexmedetomidine, is widely used for sedation in intensive care units because it has a less respiratory depressive effect.¹ In addition, several benefits of dexmedetomidine that favor its use in intensive care have been reported, such as reduced opioid dosage requirement. In animal studies, Hayashi et al reported that dexmedetomidine prevented epinephrine-induced arrhythmias in halothane-anesthetized dogs.² This antiarrhythmic effect of α_2 -adrenergic agonists may be partly ascribed to vagal activation.³ It has already been reported that central sympathetic inhibition by an α_2 -adrenergic agonist, guanfacine, augmented the sleep-related ultradian rhythm of parasympathetic tone in patients with chronic heart failure.⁴ Although α_2 -adrenergic agonists are widely recognized as inducing a vagal-dominant condition through the suppression of sympathetic nerve, there is little direct evidence that they directly increase cardiac vagal nerve activity, because such activity has been assessed only by indirect methods, such as heart rate variability,

in most studies.⁵

Vanoli et al⁶ reported that vagal stimulation after an acute ischemic episode effectively prevented ventricular fibrillation in dogs. Their group also indicated that the dogs that developed ventricular fibrillation during the acute ischemic episode had a significantly lower baroreflex-mediated heart rate response,⁷ suggesting the importance of the baroreflex in controlling vagal function. If an α_2 -adrenergic agonist is able to activate the cardiac vagal nerve directly or via modulation of the baroreflex function, it will provide a new therapeutic option for life-threatening arrhythmias after myocardial ischemia.

Medetomidine is a racemic mixture of 2 stereoisomers, dexmedetomidine and levomedetomidine. However, because it has already been reported that levomedetomidine has no effect on cardiovascular parameters and causes no apparent sedation or analgesia,⁸ the pharmacokinetics of dexmedetomidine and racemic medetomidine are almost similar. We hypothesized that medetomidine can activate the cardiac vagal nerve

Received June 1, 2011; revised manuscript received September 6, 2011; accepted September 14, 2011; released online October 29, 2011
Time for primary review: 25 days

Department of Cardiovascular Dynamics (S. Shimizu, T.K., Y.S., M.M., A.K., T.S., M.I., M. Sugimachi), Department of Cardiac Physiology (T.A., M. Shirai), National Cerebral and Cardiovascular Center Research Institute, Suita; and Department of Cardiovascular Surgery, Okayama University Graduate School of Medicine, Dentistry and Pharmaceutical Sciences, Okayama (S. Sano), Japan

Mailing address: Shuji Shimizu, MD, PhD, Department of Cardiovascular Dynamics, National Cerebral and Cardiovascular Center Research Institute, 5-7-1 Fujishiro-dai, Suita 565-8565, Japan. E-mail: shujismz@ri.ncvc.go.jp

ISSN-1346-9843 doi:10.1253/circj.CJ-11-0574

All rights are reserved to the Japanese Circulation Society. For permissions, please e-mail: cj@j-circ.or.jp

through a central action and improve the baroreflex control of vagal nerve activity. We have established a cardiac microdialysis technique for separate monitoring of neuronal norepinephrine (NE) and acetylcholine (ACh) release to the rabbit sinoatrial (SA) node in vivo.^{9–11} Using this microdialysis technique, we investigated the effects of medetomidine on cardiac autonomic nerve activities innervating the SA node.

Methods

Surgical Preparation

Animal care was provided in accordance with the “Guiding principles for the care and use of animals in the field of physiological sciences” published by the Physiological Society of Japan. All protocols were approved by the Animal Subject Committee of the National Cerebral and Cardiovascular Center.

In this study, 31 Japanese white rabbits weighing 2.3–3.0 kg were used. Anesthesia was initiated by an intravenous injection of pentobarbital sodium (50 mg/kg) via the marginal ear vein, and then maintained at an appropriate level by continuous intravenous infusion of α -chloralose and urethane ($16 \text{ mg} \cdot \text{kg}^{-1} \cdot \text{h}^{-1}$ and $100 \text{ mg} \cdot \text{kg}^{-1} \cdot \text{h}^{-1}$) through a catheter inserted into the femoral vein. The animals were intubated and ventilated mechanically with room air mixed with oxygen. Respiratory rate and tidal volume were set at 30 cycles/min and 15 ml/kg, respectively. Systemic arterial pressure was monitored by a catheter inserted into the femoral artery. Esophageal temperature, which was measured by a thermometer (CTM-303, Terumo, Japan), was maintained between 38°C and 39°C using a heating pad.

With the animal in lateral position, a right lateral thoracotomy was performed and the right 3rd to 5th ribs were partially resected to expose the heart. After incising the pericardium, a dialysis probe was implanted as described below. Three stainless steel electrodes were attached around the thoracotomy incision for recording body surface electrocardiogram (ECG). The heart rate was determined from the ECG using a cardi tachometer. Heparin sodium (100 IU/kg) was administered intravenously to prevent blood coagulation. At the end of the experiment, the animal was killed humanely by injecting an overdose of pentobarbital sodium. In the postmortem examination, the right atrial wall was resected en bloc with the dialysis probe. The inside of the atrial wall was observed macroscopically to confirm that the dialysis membrane was not exposed to the right atrial lumen.

Dialysis Technique

The materials and properties of the dialysis probe have been described previously.^{9–12} A dialysis fiber of semipermeable membrane (length 4 mm, outer diameter 310 μm , inner diameter 200 μm , PAN-1200, molecular weight cutoff 50,000; Asahi Chemical, Tokyo, Japan) was attached at both ends to polyethylene tubes (length 25 cm, outer diameter 500 μm , inner diameter 200 μm). A fine guiding needle (length 30 mm, outer diameter 510 μm , inner diameter 250 μm) with a stainless steel rod (length 5 mm, outer diameter 250 μm) was used for the implantation of the dialysis probe. A dialysis probe was implanted into the right atrial myocardium near the junction of the superior vena cava and the right atrium. After implantation, the dialysis probe was perfused with Ringer’s solution (in mmol/L: NaCl 147, KCl 4, CaCl₂ 3) containing a cholinesterase inhibitor eserine (100 $\mu\text{mol/L}$), at a speed of 2 $\mu\text{l/min}$ using a microinjection pump (CMA/102, Carnegie Medicin, Sweden). Experimental protocols were started 120 min after implantation of the dialysis probe. The dead space between the dialysis membrane and the sample tube was taken into account at the beginning of

each dialysate sampling. In protocols 1 and 2 as described below, 8 μl of phosphate buffer (pH 3.5) was added to each sample tube before dialysate sampling, and each dialysate sampling period was set at 20 min (1 sample volume=40 μl). Half of the dialysate sample was used for ACh and the other half for NE measurements. In protocol 3, 2 μl of phosphate buffer was added to each sample tube before dialysate sampling, and each dialysate sampling period was set at 5 min (1 sample volume=10 μl). In protocol 4, 4 μl of phosphate buffer was added to each sample tube before dialysate sampling, and each dialysate sampling period was set at 10 min (1 sample volume=20 μl). Dialysate NE and ACh concentrations were analyzed separately by high-performance liquid chromatography as described previously.^{12,13}

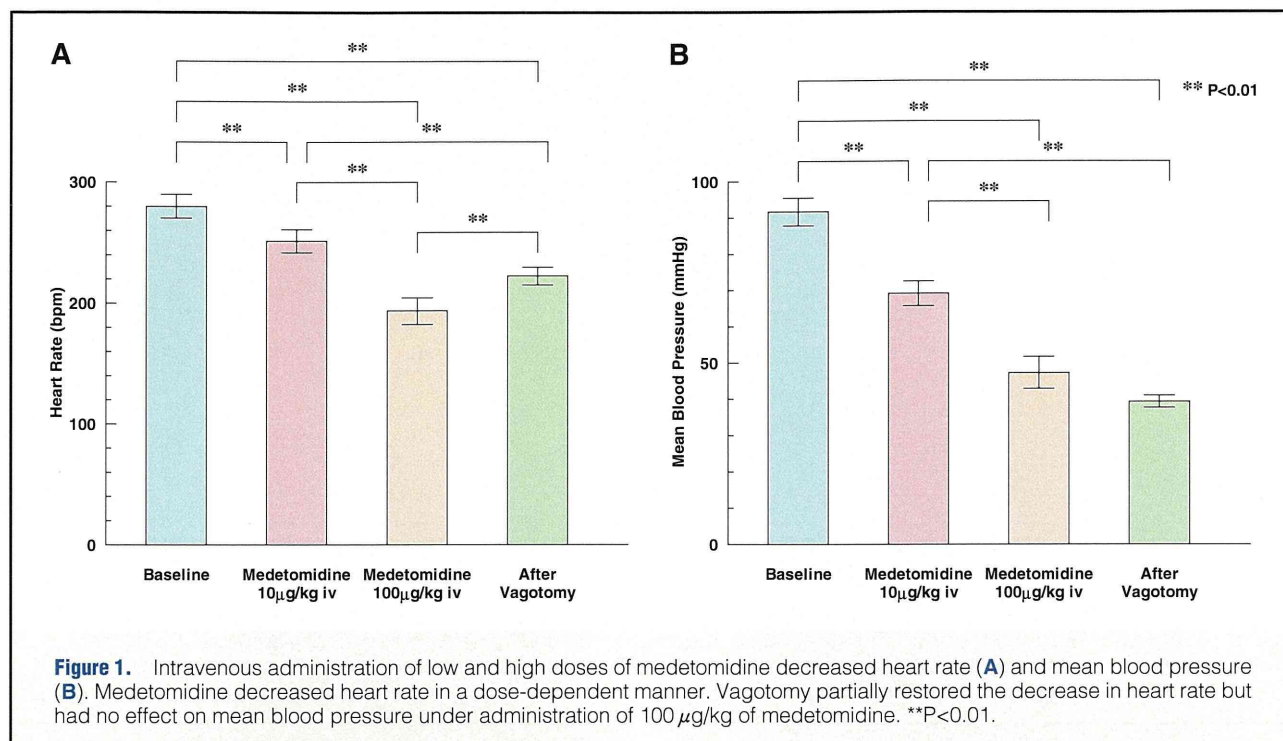
Experimental Protocols

Protocol 1 (n=7) Baseline dialysate was sampled before the injection of medetomidine. Thereafter, a low dose (10 $\mu\text{g/kg}$) of medetomidine was injected intravenously via the femoral vein. After allowing 20 min for hemodynamic stabilization, dialysate was sampled for 20 min (40 μl). When the hemodynamics had recovered to the baseline level, a high dose (100 $\mu\text{g/kg}$) of medetomidine was injected intravenously and another 20-min dialysate sample was collected after hemodynamic stabilization. Finally, the vagal nerves were sectioned bilaterally at the neck and a dialysate sample was collected immediately after vagotomy. In 4 rabbits, an α 2-adrenergic antagonist, atipamezole (2.5 mg/kg), was intravenously administered before euthanasia and hemodynamic responses were recorded.

Protocol 2 (n=7) To prevent possible interference of medetomidine-induced hypotension with vagal nerve activity, intravenous infusion of an α 1-adrenergic agonist, phenylephrine, was started simultaneous to intravenous injection of medetomidine. Baseline dialysate sample was collected for 20 min before medetomidine injection. Simultaneous to intravenous injection of high-dose (100 $\mu\text{g/kg}$) medetomidine, intravenous infusion of phenylephrine was started ($6.6 \pm 1.2 \mu\text{g} \cdot \text{kg}^{-1} \cdot \text{min}^{-1}$) to maintain the mean blood pressure (BP) at baseline level. After hemodynamic stabilization, dialysate was sampled for 20 min. Finally, dialysate was again sampled immediately after bilateral vagotomy.

Protocol 3 To investigate the effect of medetomidine on baroreflex-induced vagal ACh release, we varied the mean BP by changing the dose of intravenous phenylephrine in both the control (n=5) and medetomidine-treated (n=7) groups. In the control group, Ringer’s solution was infused intravenously at $1.0 \text{ ml} \cdot \text{kg}^{-1} \cdot \text{h}^{-1}$ throughout the experiment. In the medetomidine-treated group, medetomidine was initially injected intravenously at a dose of 60 $\mu\text{g/kg}$, and thereafter continuously infused at a dose of 60 $\mu\text{g} \cdot \text{kg}^{-1} \cdot \text{h}^{-1}$ or a rate of $1.0 \text{ ml} \cdot \text{kg}^{-1} \cdot \text{h}^{-1}$. After baseline dialysate sampling, mean BP was increased in a stepwise manner by altering the dose of intravenous phenylephrine (maximal dose: $32.2 \pm 5.5 \mu\text{g} \cdot \text{kg}^{-1} \cdot \text{min}^{-1}$ in the control group and $18.6 \pm 2.1 \mu\text{g} \cdot \text{kg}^{-1} \cdot \text{min}^{-1}$ in the medetomidine-treated group). Dialysate samples were collected for 5 min at 4–7 different mean BP levels. Relations of log ACh concentrations vs. mean BP were plotted and regression lines for each animal were calculated.

Protocol 4 (n=5) We investigated the peripheral effects of medetomidine on heart rate and dialysate ACh concentration under electrical stimulation of the right cervical vagal nerve. Bilateral vagal nerves were exposed through a midline cervical incision and sectioned at the neck. A pair of bipolar stainless steel electrodes was attached to the efferent side of the



right vagal nerve. The nerve and electrode were covered with warmed mineral oil for insulation. After the baseline dialysate sampling, the right efferent vagal nerve was stimulated at the frequency of 20 Hz by a digital stimulator (SEN-7203, Nihon Kohden, Japan). The pulse duration and amplitude of nerve stimulation were set at 1 ms and 10 V. Thereafter, a low dose (10 µg/kg) of medetomidine was injected intravenously via the femoral vein. After hemodynamic stabilization, dialysate was sampled for 10 min under the 20-Hz electrical stimulation of vagal nerve. Finally, a high dose (100 µg/kg) of medetomidine was injected intravenously and another 10-min dialysate sample was collected under the 20-Hz electrical stimulation.

Statistical Analysis

All data are presented as mean ± standard error. Heart rate and mean BP were compared by 1-way repeated measures analysis of variance (ANOVA) followed by a Tukey's test.¹⁴ Dialysate NE and ACh concentrations were also compared by 1-way repeated measures ANOVA followed by a Tukey's test. Comparisons of data between protocols 1 and 2 were conducted using unpaired t-test (Student's or Welch's t-test). In protocol 3, the average slopes and intercepts of the regression lines were compared using unpaired t-test. Differences were considered significant at P<0.05.

Results

Protocol 1

Intravenous injection of medetomidine significantly decreased heart rate (Figure 1A) and mean BP (Figure 1B) in a dose-dependent manner (280±10 beats/min and 92±4 mmHg, respectively, at baseline; 251±10 beats/min and 69±3 mmHg at 10 µg/kg; and 193±11 beats/min and 47±4 mmHg at 100 µg/kg, P<0.01 for all comparisons). Vagotomy increased heart rate to 222±7 beats/min but did not affect mean BP (Figures 1A,B).

Low-dose medetomidine significantly decreased dialy-

sate NE concentration (Figure 2A) from 0.72±0.06 to 0.59±0.04 nmol/L (P<0.01) but did not affect dialysate ACh concentration (Figure 2B) compared with baseline. High-dose medetomidine also decreased dialysate NE concentration (to 0.52±0.05 nmol/L) similar to low-dose medetomidine (Figure 2A) and significantly increased dialysate ACh concentration from 7.2±1.3 nmol/L at baseline to 12.1±1.6 nmol/L (P<0.01, Figure 2B). Dialysate NE concentration was not changed by vagotomy, whereas dialysate ACh concentration recovered to the baseline level immediately after vagotomy (Figures 2A,B).

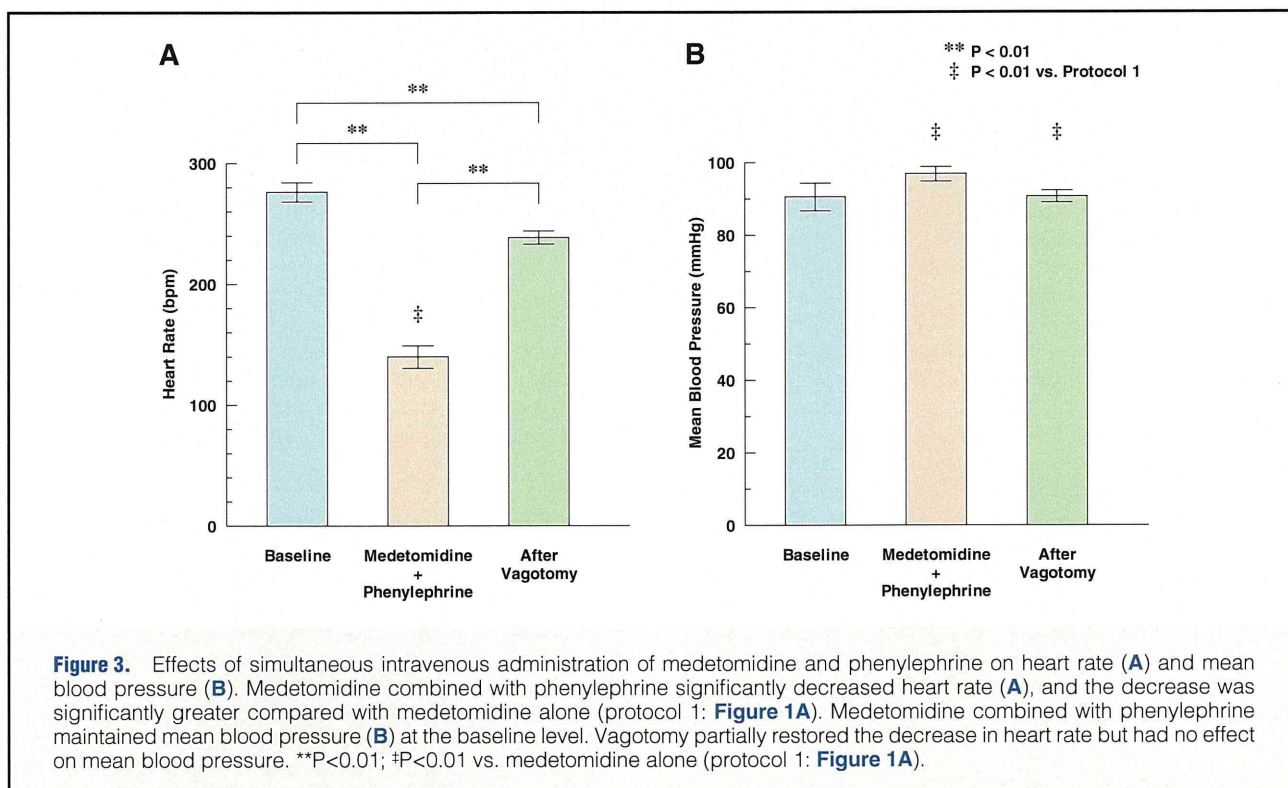
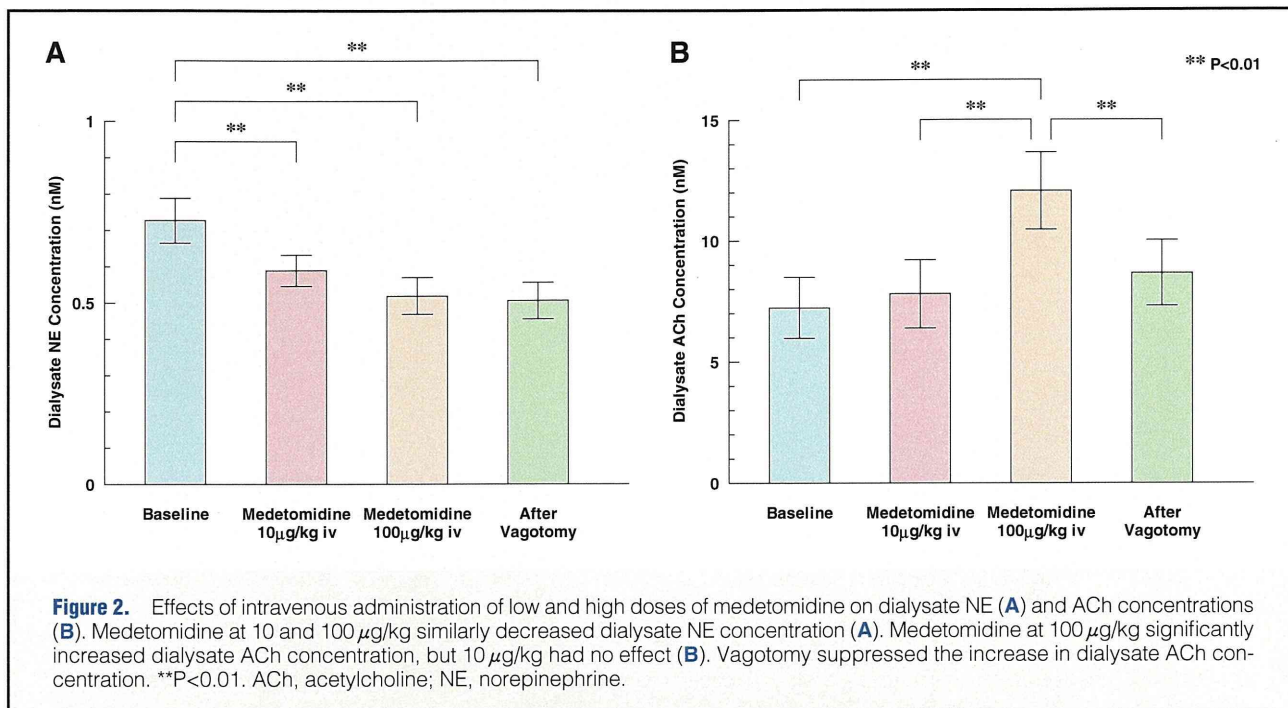
In 4 rabbits treated with atipamezole, heart rate and mean BP recovered to the baseline levels immediately after the injection (276±18 beats/min and 88±6 mmHg, respectively, at baseline; and 280±11 beats/min and 83±6 mmHg after the injection).

Protocol 2

Intravenous injection of high-dose medetomidine combined with phenylephrine decreased heart rate (Figure 3A) and the decrease was significantly greater than that observed in protocol 1 (140±9 vs. 193±11 beats/min, P<0.01), while mean BP was maintained at the same level as baseline (Figure 3B). Medetomidine combined with phenylephrine decreased dialysate NE concentration from 0.85±0.09 at baseline to 0.68±0.10 nmol/L (Figure 4A), and the decrease was not significantly different from that of medetomidine alone (protocol 1). However, medetomidine combined with phenylephrine increased dialysate ACh concentration (Figure 4B) to a significantly and markedly higher level than that observed in protocol 1 (26.8±5.4 vs. 12.1±1.6 nmol/L, P<0.05). Dialysate ACh concentration recovered to the baseline level immediately after vagotomy.

Protocol 3

The change in mean BP by phenylephrine administration affected dialysate ACh concentration only slightly in the control group (Figure 5A), whereas the elevation of mean BP



markedly increased dialysate ACh concentration in the medetomidine-treated group (Figure 5B). The average slopes of the regression lines between mean BP and log dialysate ACh concentration were 0.0018 ± 0.0004 in the control and 0.0062 ± 0.0006 in the medetomidine-treated group. The slope was significantly steeper in the medetomidine-treated group than that in the control ($P < 0.01$). However, the intercept did not differ significantly between the control (0.59 ± 0.05) and

medetomidine-treated (0.68 ± 0.07) groups.

Protocol 4

The 20-Hz electrical stimulation of the right vagal nerve significantly decreased heart rate from 271 ± 11 beats/min at the baseline to 112 ± 6 beats/min and increased dialysate ACh concentration from 7.1 ± 0.9 nmol/L at the baseline to 38.5 ± 7.2 nmol/L ($P < 0.01$). However, both 10 and 100 μg/kg of me-